TU Delft Delft University of Technology

Engineering Critical Assessment of Buckle Arrestor

Master Thesis

Ning Wu

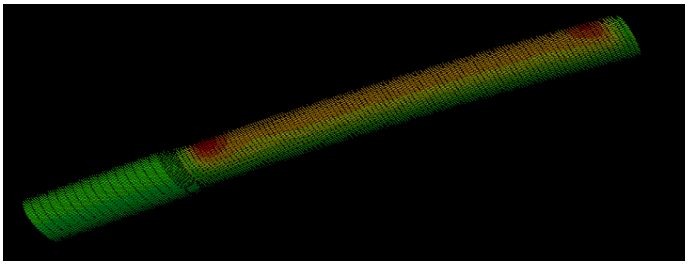

Supervisor
Prof.Dr.A.V.Metrikine
Dr.Ping Liu
Dr.ir.Michael Janssen
Dr.ir.F.P.van der Meer

INTECSEA
WorleyParsons Group

Abstract

In the deep water S-lay installation, the buckle arrestor rolls on and drops off the rollers repeatedly when it moves along the stinger. When the buckle arrestor is located on the roller, there is strain intensification at the 12 o'clock position of the pipe section which is close to the buckle arrestor, and the strain can reach 1%. When the buckle arrestor drops off the roller, the strain decreases. The maximum strain occurs around the position where the girth welding is located, a defective girth welding part may fail under this cyclic loading. If an initial flaw exists, it is important to be able to predict the total crack growth under the cyclic loading process.

The thesis is conducted in three stages. In the first stage, the global FE model is used to model the buckle arrestor behavior during its passage over the stinger, especially the bending moment variation. In the second stage, the output from the global model is used as input for the local FE model, to obtain the stress and strain of the pipe cross section. In the third stage, based on the local output, Engineering Critical Assessment is carried out on the girth welding part. The girth welding safety is judged by comparing the predicted crack growth with the limit standard.

It is found out that the buckle arrestor is safe under realistic cyclic loading conditions. This is due to the relatively small strain range which causes little influence on the fracture resistance. The total crack growth can be treated as superposition of tearing growth and fatigue growth.

While when large cyclic strain range is applied, according to some experiments and numerical results, the simplified superposition method is not suitable anymore. The compressive loading could reduce the crack tip fracture resistance. In that case, a proper evaluation of the fracture resistance under the large cyclic loading conditions becomes necessary. Further systematic study should be carried out on the mutual effects of tearing growth and fatigue growth.

Contents

Notation

CTOD	Crack Tip Opening Displacement
K	Stress Intensity Factor
E	Young's modulus
σ_t	True stress
ε_t	True strain
K_{mat}	Critical Stress Intensity Factor
δ_{mat}	Fracture toughness in terms of CTOD
L_r	Load ratio
σ_{ref}	Reference stress
σ_y	Yield stress
K_r	Fracture ratio
$K_{I,p}$	Applied stress intensity factor due to primary loads
$K_{I,s}$	Applied stress intensity factor due to secondary loads
ΔK	Stress intensity factor range
ρ	Plastic interaction effect
ECA	Engineering Critical Assessment

Chapter 1

Introduction

1.1 General Background

The applications of offshore pipeline gradually move towards ultra deep water, a considerable amount of work needs to be done to ensure pipeline safety during fabrication, installation and operation phases. These force engineers to deepen the development in the design stage. In the engineering industry, some standard codes like the DNV-OS-F101 have published the relevant limit state design criterion. The marine pipeline system should be designed against these potential failure modes: Serviceability Limit State, Ultimate Limit State, Fatigue Limit State, Accidental Limit State [3].
-Serviceability Limit State describes a condition, if exceed, the pipeline normal operations will be influenced. Usually it emphasizes on local damage, unacceptable deformations, etc.
-Ultimate Limit State represents a situation, if exceed, the integrity of the pipeline will be destroyed. For instance, bursting, plastic collapse, etc.
-Fatigue Limit State means the fatigue crack growth of a structure under cyclic loading.
-Accidental Limit State describes excessive pipeline damage as a result of accidents, like dragging anchors, extreme waves, etc.

The South Stream Transport B.V. is planning to build a new gas pipeline system across the Black Sea. The pipeline system contains four offshore 32-inch pipelines. The total length is about 930 km. The maximum water depth reaches 2200 m.

1.2 Objective of Thesis

In order to avoid the pipeline from buckling, especially in deep water section, every 2000 m a buckle arrestor is positioned. During the S-Lay installation phase, the buckle arrestor will pass over the stinger, it goes on and drops off the roller-boxes in several cycles. When the buckle arrestor is located on the roller-box, at 12 o'clock position of the pipe section which is close to the buckle arrestor, there will be strain intensification. Especially when the water depth reaches 2200 m, the local strain is quite high and can approach nearly 1%. When the buckle arrestor drops off the

roller-box, due to the unloading, the strain intensification reduces.

The strain intensification area is the position where the girth welding is located, as illustrated in Figure 1.1. In reality, the welding part is not perfect, flaws already exist. Thus in this situation, the buckle arrestor passes over the roller-boxes repeatedly, the girth welding part will experience the cyclic loads. If there is a surface flaw at 12 o'clock position of the girth welding part, under these cyclic loadings, the final crack growth may exceed the allowable limit. For instance, the maximum allowable crack growth is 1 mm. Once it exceeds, it will be dangerous for the following installation and the future operation activities.

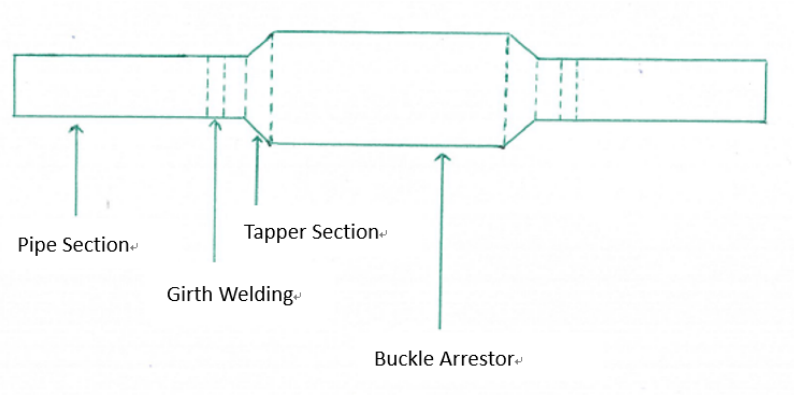

Figure 1.1: Sketch of the buckle arrestor

Detailed analysis must be carried out to predict the total crack growth under the cyclic loading history. First, the cyclic loads on the buckle arrestor during its passage over the stinger will be evaluated properly. Then according to the identified loads, the Engineer Critical Assessment is carried out on the defective girth welding part. The predicted total crack growth is compared with the limit standard. If it is within the limit state, then the buckle arrestor is safe. If it exceeds the allowable crack growth, the buckle arrestor will be dangerous, further work need to be done in the pipeline design phase.

1.3 Method of Thesis

The global analysis is conducted in the first stage, the FE modeling is used to identify the buckle arrestor global behaviors. The typical static FE modeling is reproduced. Also a modified FE model is created to investigate the stress, the strain and the bending moment variations under the proper time loading history.

Because of the beam element type, the mesh size and the model scale, the global FE model could not catch the pipe cross section behavior. Therefore a local FE model is created in the second stage. The model scale is reduced, the local geometry is specified, the 3D solid element is used, and the mesh size is refined. The global output will be used as input for the local FE model to obtain the local strain and stress.

In the third stage, based on the obtained local strain and stress, the Engineering Critical Assessment is carried out on the girth welding part. Both ductile tearing and fatigue growth are evaluated to predict the total crack growth. According to the previous similar FE research and experiments study, the predicted crack growth is compared with the limit standard.

Chapter 2

Global S-Lay Installation Analysis

2.1 S-Lay in OFFPIPE

2.1.1 General Introduction

In deep water pipeline S-Lay installation, the required curvature of stinger section is quite high, and the departure angle could reach to 70 ° or even more. The departure angle means the angle when pipe slides off the stinger, usually the second to last roller. The objective of the large departure angle is to avoid over-high strain intensification on the pipe at the departure roller-box. When pipe follows the high stinger curvature, the overall high top tensile strain increase plastic deformation at 12 o'clock location [11]. And the discontinuous roller-boxes support reactions increase the pipe local curvature which lead to higher local bending moment. As a result, the local strain of the pipe at the support positions are much higher than other locations. Figure 2.1 and Figure 2.2 are examples that illustrate the phenomenon. Some industry criteria like DNV OS F-101, ASME VII, have defined the relevant limit states criterion for the over-bend strain to insure the safety during installation phase.

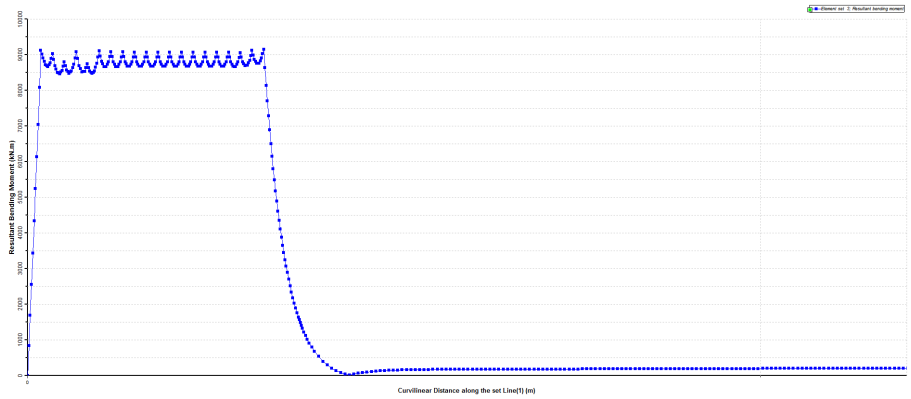

Figure 2.1: Bending Moment Variation of S-Lay

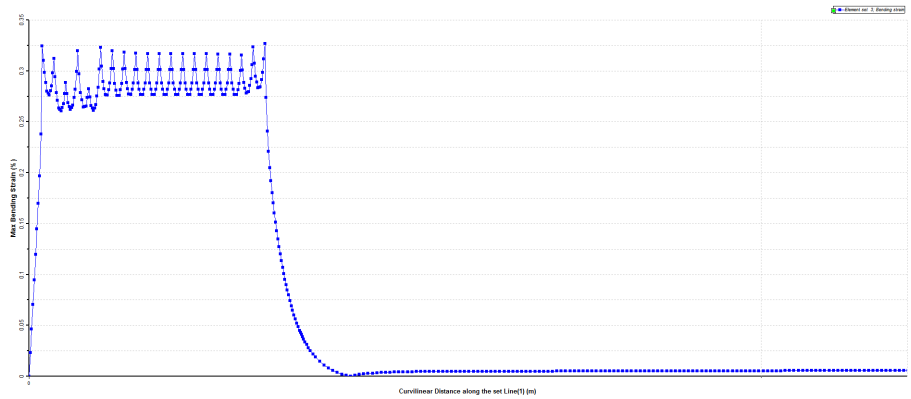

Figure 2.2: Bending Strain in S-Lay

2.1.2 Case Study

OFFPIPE is a classical software to model offshore pipeline installation and operation. It is based on the nonlinear finite element method. The classical Euler-Bernoulli beam theory is used to analyse offshore pipeline and cable structures, including static and dynamic situations.

The case study is based on the South-Stream Project. Static analyses of the 2200 m water depth S-Lay are performed in the OFFPIPE(2.06). The pipe diameter is 32-inch and the wall thickness is 39 mm. The steel material grade is $X65$ and the concrete coating is neglected. The singer radius is 140 m, and the fixed-end beam element is used to model the stinger. The stinger geometry is defined by specifying x coordinate and y coordinate of the stinger nodes explicitly. Three dimensional simple support is used to restrain pipe lateral displacement. And the support property is presented by defining the roller stiffness.

According to the definition of the OFFPIPE, the roller-bed length means the effective contact length between pipe face and roller-box face. Three cases are investigated based on the different roller-bed lengths, including single node support, roller-bed length of 1 m, roller-bed length of 7 m which nearly covers the whole span between two stinger nodes. The Figure 2.3 illustrates them.

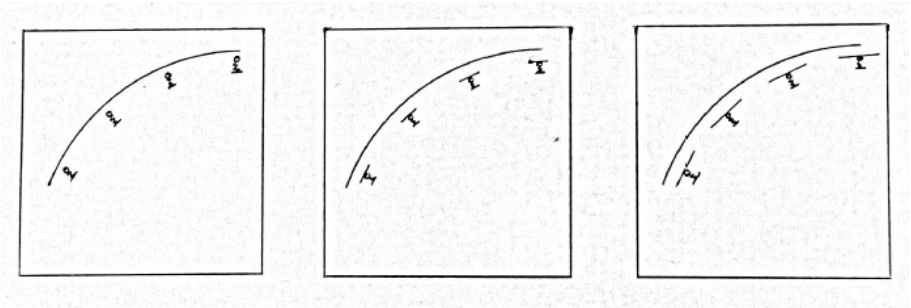

Figure 2.3: Roller-boxes Modes

Static analyses have been carried out on these three modes. The bending moments

and strains at the stinger nodes of these three cases are shown in Table 2.1 and Table 2.2 respectively. According to the results, increasing the roller-bed contact length could reduce the local bending moment and strain concentration. At the departure roller-box, the moment is highest. Especially when the support reaction become a single node force, the strain could reach 0.414%. This strain is quite high and the fracture assessment should be carried out [3]. This feature has been proved in many practical S-Lay projects, especially in deep water installation. By covering the span between two roller-boxes to increase the contact area, lower strain concentration will appear on the pipe section.

Table 2.1: Bending Moment Variations along Stinger Nodes

Bending Moments (kN.m)			
tinger Nodes	Roller-bed Length(0 m)	Roller-bed Length(1 m)	Roller-bed Length(7 m)
1	9468.5	9386.6	8878.9
2	9048.9	9005.3	8734.5
3	9138.9	9081.2	8723.4
4	9056.3	9005.2	8688.3
5	9242.8	9181.6	8802.1
6	9107.7	9056.4	8738.4
7	9129.5	9075.9	8743.9
8	9092.3	9039.4	8711.1
9	9112.6	9058.1	8719.9
10	9075.4	9025.4	8715.3
11	9207.2	9148.5	8784.6
12	9246.4	9183.9	8821.5
13	9076.2	9026.5	8783.4
14	9473.5	9351.9	8652.7
15	4868.3	4868.3	4868.3
16	2523.7	2523.7	2523.7
17	1308.5	1308.5	1308.5

2.2 FE Global Modeling

2.2.1 Base Model

General

In deep water pipeline installation, in order to prevent pipe from buckling, within a certain length, a buckle arrestor is positioned. When the buckle arrestor passes over the stinger, due to the increase of wall thickness, the reaction force will be higher when the buckle arrestor is positioned on the roller-box. As a result, the

Table 2.2: Total Strain Variations along Stinger Nodes

Total Strains (%)			
tinger Nodes	Roller-bed Length(0 m)	Roller-bed Length(1 m)	Roller-bed Length(7 m)
1	0.414	0.399	0.332
2	0.351	0.345	0.318
3	0.362	0.354	0.317
4	0.351	0.345	0.314
5	0.376	0.368	0.324
6	0.358	0.351	0.318
7	0.360	0.353	0.318
8	0.356	0.349	0.316
9	0.358	0.351	0.317
10	0.353	0.347	0.316
11	0.371	0.363	0.322
12	0.376	0.367	0.326
13	0.353	0.347	0.318
14	0.414	0.393	0.310
15	0.170	0.170	0.170
16	0.105	0.105	0.105
17	0.072	0.072	0.072

local bending moment increases with respect to the average bending moment of the pipe sections. Higher strain intensification will appear at 12 o'clock position of the pipe sections which are close to the buckle arrestor. And that is the place where girth welding part is located. Detailed analysis must be carried out to ensure that the strain intensification will not exceed the allowable value.

Several numerical studies have been carried out on this phenomenon. Typically, by replacing part of the pipe section with the buckle arrestor at the certain location which corresponding to the roller-box under investigation. Then external loads are added to let them follow the stinger profile. Usually the departure roller position where the maximum strain intensification appears is assessed. If the strain satisfies the fracture assessment, the pipe is considered safe.

However, the strain intensification area is the place where girth welding is located. In reality, defects exist in the girth welding before installation. During installation, the buckle arrestor goes on and drops off the roller-boxes repeatedly. Especially if some emergencies happen, the pipeline will be pulled back, more cycles will be suffered. Under these cyclic loadings, the crack will grow. It will be very dangerous if the final crack growth exceeds the safety standard.

Geometry

Based on the typical way of modeling the buckle arrestor, a simplified model is created in Abaqus(6.14). The pipe and the buckle arrestor are modeled with the 2-nodes beam elements(B21), the cross section properties are presented in Table 2.3, thick wall pipe is adopted. The steel grade is X65, and the material is elastic-perfect plastic. The true stress-strain curve is used in the analysis. And the steel density will be used in gravity.

Table 2.3: Pipe Section Properties

	Pipe Section	Tapper Section	Buckle Arrestor
Diameter	0.8128 m	0.8478 m	0.8828 m
Wall Thickness	0.039 m	0.057 m	0.074 m
Length		0.14 m	3.32 m

The stinger profile is modeled under a perfect radius of 140 m, nearly every 8 m along the circumference a roller-box is positioned. Seven roller-boxes are taken into account, they are modeled as the rigid circles with the radius of 0.3 m. As for the contact properties, in the tangent direction, it is frictionless; in the normal direction, a linear contact stiffness of 70000 kN/m is assigned.

Boundary Conditions

For the boundary conditions, the rollers are completely fixed, no displacements and rotations are allowed. The right end of the pipe is totally fixed, external loads are added on the left end, as present in Figure 2.4.

Loading Steps

First, the tension of 7000 kN is added on the left end of pipe, and it is allowed to follow the rotation in the following loading steps.

Second, according to the departure angle, the equivalent rotation angle is added on the left end of pipe, mainly to let pipe fit the stinger profile. The magnitude of the tension will not be changed, while its direction will follow the rotation.

Third, the effective gravity forces are added on different sections. Because the model is built up under Standard/Explicit Model, the static buoyancy can not be added directly. Assuming that the empty pipe sections are fully submerged in water, gravity and buoyancy are combined together by calculating the effective accelerations of pipe sections, tapper sections, and buckle arrestor respectively. The calculation methods are described below.

Weight per unit length in air:

$$W_{air} = \pi * \left(\left(\frac{D_o}{2} \right)^2 - \left(\frac{D_o - 2t}{2} \right)^2 \right) * \rho_{steel}$$

Submerged Weight per unit length:

$$W_{sub} = W_{air} - \rho_{sea} * g * \pi * \left(\frac{D_o}{2} \right)^2$$

Mass per unit length:

$$M = \frac{\pi}{4} * D_o^2 - (D_o - 2t)^2 * \frac{\rho_{steel}}{g}$$

Effective acceleration:

$$g_{eff} = \frac{W_{sub}}{M}$$

Here D_o is the outside diameter, t is the wall thickness.

In order to model the pipe sections conveniently, the whole stinger profile has been rotated 17 ° in clockwise direction at the beginning. The reason is that, the model is made reference from a pipe-lay vessel, under the global coordinate, the tangential direction of the first roller is not in horizontal. While the effective gravity is added under the local coordinate. So the obtained effective accelerations which is based on the global coordinate must be decomposed in x-direction and y-direction respectively. The tension and rotation are maintained the same. The decomposed effective accelerations are added in the third stage.

Base Case

In order to avoid the influence of the pipe right end boundary conditions, the investigated positions start from the third roller to the sixth roller which corresponding to the departure roller. The buckle arrestor is positioned on these rollers and between these rollers respectively. Examples are presented in Figure 2.4 and Figure 2.5.

2.2.2 Modeling with Time Loading History

When the buckle arrestor passes over the stinger, it goes on and drops off the roller-boxes repeatedly. In order to study its behavior under the cyclic loading situation, a new model is developed by modifying the base model.

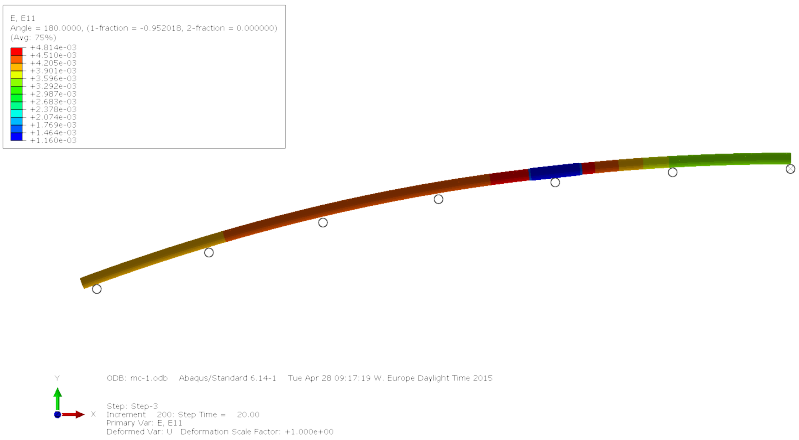

Figure 2.4: Buckle Arrestor on the Third Roller

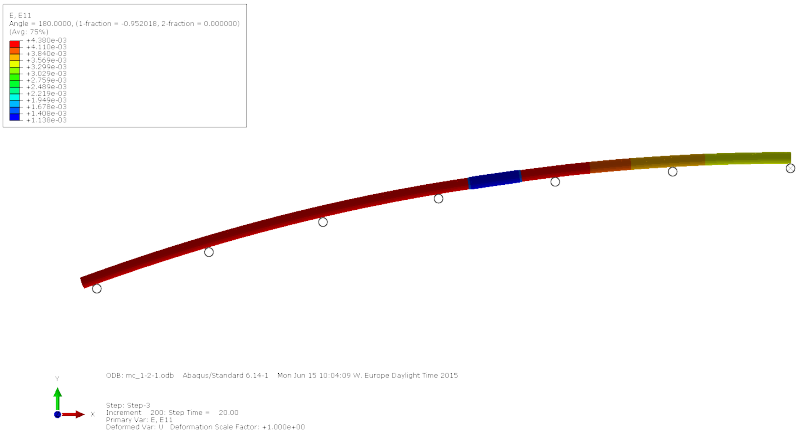

Figure 2.5: Buckle Arrestor between the Third and the Fourth Roller

First Step

The pipe sections with the buckle arrestor are maintained at unloading state. A supplementary pipe section is added on the right side of the first roller, see in Figure 2.6. This supplementary section is restricted by a group of fixed rollers which are located at both top and bottom positions. Similarly when defining the contact properties of these rollers, in the tangent direction, it is frictionless; in the normal direction, the contact stiffness is 70000 kN/m. The main objective of these rollers is to restrict the vertical displacements and rotations of the supplementary section when the buckle arrestor moves along the stinger. The right end of feeding section is restrained in the displacement of y-direction. The rotation around z-axis is restrained as well. So the supplementary section is allowed to move only in x-direction during later loading steps.

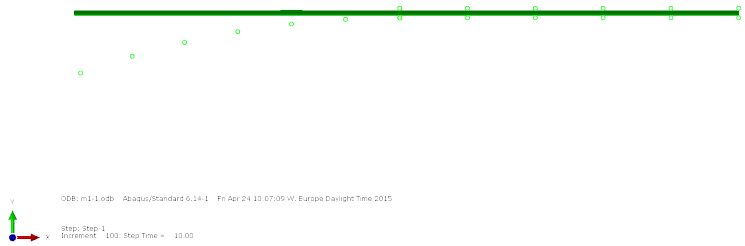

Figure 2.6: Initial State

Second Step

The procedures are similar to the base model. The tension, rotation and effective gravity are applied step by step. The pipe sections is draped on the stinger, see the Figure 2.7

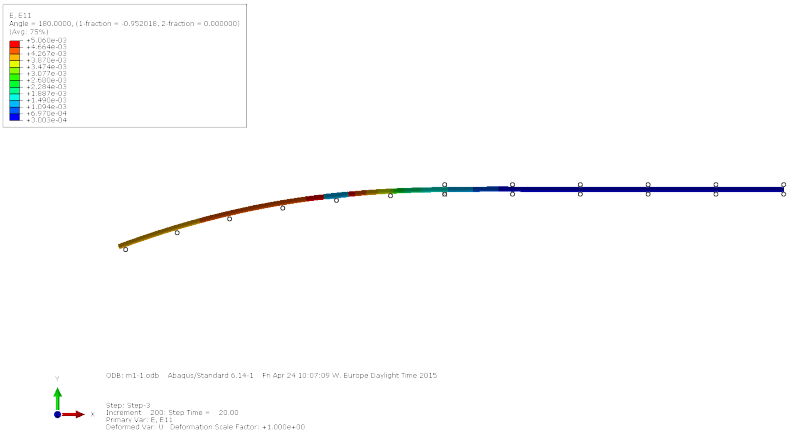

Figure 2.7: Drape Pipe on Stinger

Third Step

The buckle arrestor is forced to move along the stinger profile under proper time loading history. At the left end, the original draped pipe slides off the stinger. At the right end, new pipe sections are continuously supplemented. The procedure looks like installing pipe.

Both loading control method and displacement control method have been applied. Through the simulation, it was found out that the loading control method is not

appropriate. Because it is hard to adjust the balance between tension and bending moment. As a result, the buckle arrestor could not follow the stinger profile properly. So the displacement control method is adopted here, the mainly objective is to maintain the curvature of pipe sections during its passage over the stinger.

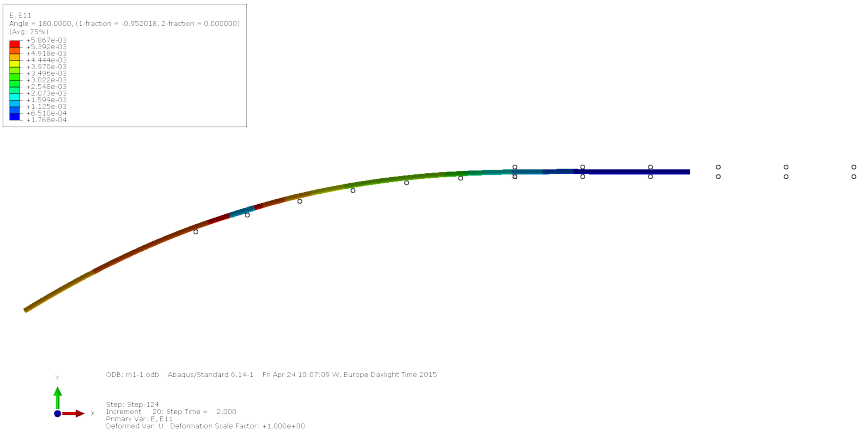

Figure 2.8: Buckle Arrestor Move to the Departure Roller

During the simulation, every 2s, the right end of pipe is moved 0.2 m towards left direction. Meanwhile, the rotation angle at the pipe left end is increased by 0.0015 radians, mainly to maintain the departure angle. Under this loading procedure, the buckle arrestor moves along the stinger profile smoothly. It goes on the rollers and drops off the rollers step by step till the departure roller, as shown in Figure 2.8. According to the results in Figure 2.8, the strain at the supplementary section is really small which means that it has hardly any influence on the buckle arrestor part, so the modeling method is reasonable.

2.2.3 Simulation Results

Base Model

Several cases have been performed, the buckle arrestor is positioned on different locations. Figure 2.9 and Figure 2.10 are examples which show the longitudinal strain variation along the pipe sections when the buckle arrestor is located on the roller and between the rollers respectively.

When the buckle arrestor is located on the rollers, at the both side of the buckle arrestor, there are strain intensification on the pipe sections. The largest strain intensification appears at the sixth roller. While when buckle arrestor is located between the rollers, the strain intensification reduces. The relevant strain values of these two situations are summarized in Table 2.4.

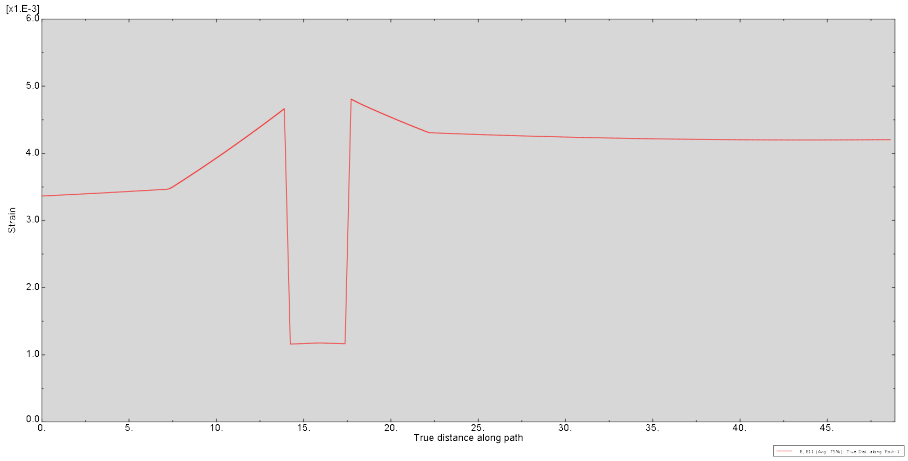

Figure 2.9: Strain Variation-Buckle Arrestor on the Third Roller

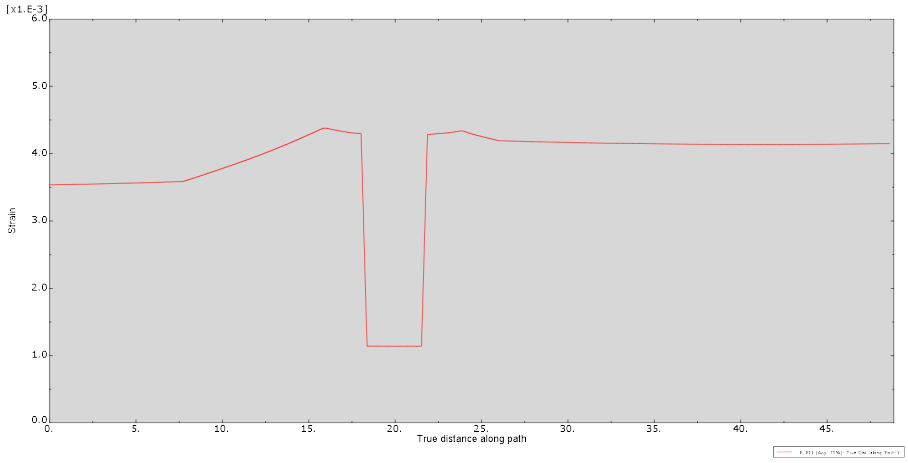

Figure 2.10: Strain Variation-Buckle Arrestor between the Third and Fourth Rollers

Table 2.4: Strain at Girth Welding Part

On the rollers	3rd	4th	5th	6th
Strain (%)	0.48	0.48	0.48	0.5
Between the Rollers	3rd-4th	4th-5th	5th-6th	
Strain (%)	0.43	0.43	0.43	

Moving Model

The simulation results are presented as follows. Figure 2.11 shows the strain variation of a element which is selected from the strain intensification area under the time loading history.

As reflected from the graph, the strains almost keeps the same level when the buckle arrestor moves on the rollers or moves between rollers respectively. These also reflect that added loading history is reasonable since it maintains appropriate curvatures of the buckle arrestor. When the buckle arrestor is located on the sixth roller, the

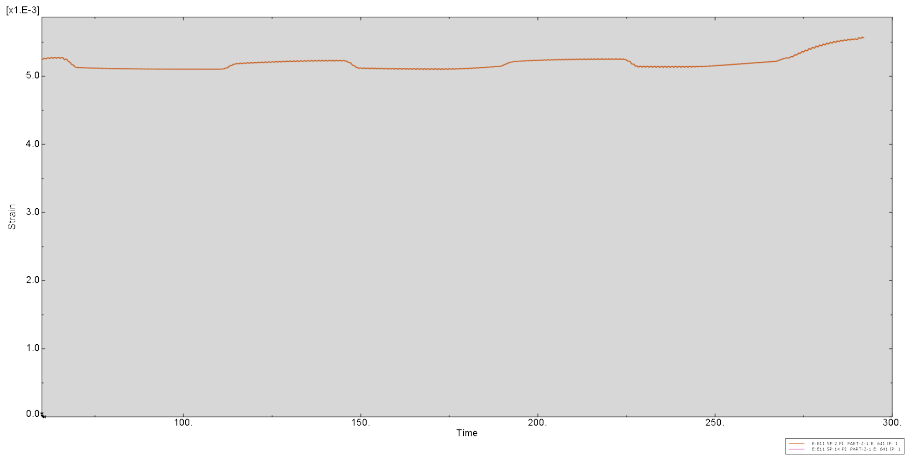

Figure 2.11: Longitudinal Strain(Girth Welding) under Time Loading History

strain will be higher. Table 2.5 summarizes the results.

Table 2.5: Strain at Girth Welding Part

On the rollers	3rd	4th	5th	6th
Strain (%)	0.52	0.52	0.52	0.55
Between the Rollers	3rd-4th	4th-5th	5th-6th	
Strain (%)	0.5	0.5	0.5	

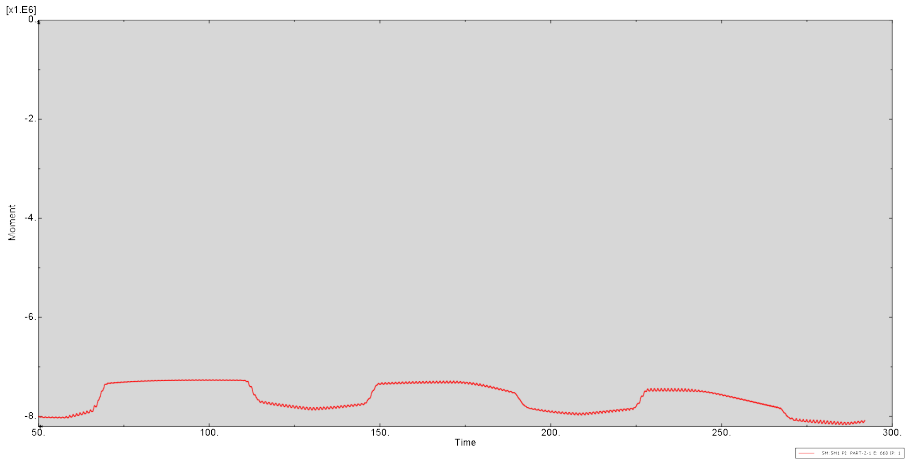

Figure 2.12: Bending Moment(Buckle Arrestor Mid Point) under Time Loading History

Figure 2.12 presents the bending moment variation of a element which is picked from the middle of the buckle arrestor under the time loading history. When the buckle arrestor is located on the roller, the bending moment maintains around 8100 kN.m;

when it is between the rollers, the bending moment drops to about 7000 kN.m. At the departure roller, the moment is bit higher, it is around 8200 kN.m. The bending moment variation will be used in local FE analysis.

Comparing the results of these two models, the moving model is more conservative. The possible reasons are: in the new model, the total fixed end is away from the first roller; the gravity effects of the feeding pipe sections; in order to let the buckle arrestor follow the stinger path, the displacement control is added strictly.

A good advantage of the new model is that, the time loading history will give better estimation of the cyclic loading is quite large. Especially accessing the strain when buckle arrestor between the roller-boxes, the strain will be smaller if it neglects residual strain which caused by previous plastic deformation.

Chapter 3

Buckle Arrestor Local FE Analysis

3.1 Static Modeling Analysis

3.1.1 Former Study

In the global model, 2D beam elements are used, mainly to obtain the global bending moment, roller reaction forces, etc. However it could not reflect the local strain/stress behavior of pipe cross section. So a more specific local FE model has to be made to identify the detail strain/stress behavior of pipe. The local analysis results will be used in fracture assessment.

According to the study from Saipem S.p.A [1], a whole buckle arrestor with sufficient extended pipe sections is built. The FE model is used for the situation when buckle arrestor on the rollers. By adding global output into local the FE model, more specific strain intensifications along the pipe sections are obtained. It turns out that the longitudinal strain intensifications in both left and right sides are almost the same [1], as shown in Figure 3.1.

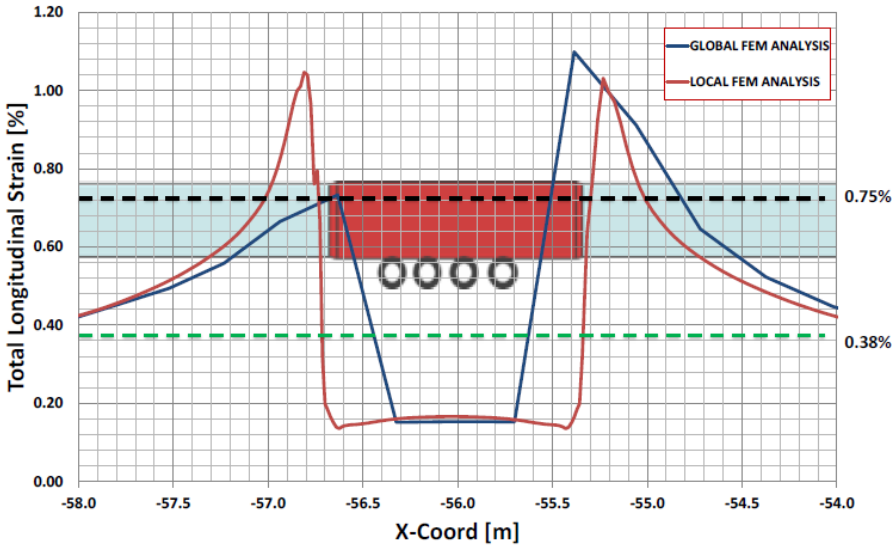

Figure 3.1: Longitudinal Strain Along Buckle Arrestor [1]

3.1.2 Simplified Model

Based on the previous study, the symmetry characteristic is considered, and half of the buckle arrestor with extended pipe is modeled. The pipe section must be sufficient so that the boundary conditions of the pipe end will not influence the strain intensification area. In the local FE model, detailed geometry is considered, tapper section is added between buckle arrestor and pipe section. Solid C3D8R element is used here, and the model is detail meshed in order to grasp the strain intensification behavior.

The global output can be used as input of local model, tension and bending moment are added at the end of buckle arrestor. The dynamic amplification effect is considered. In a conservative way, 10200 kN.m bending moment is added for the situation when the buckle arrestor is located on the rollers. When the buckle arrestor is positioned between the rollers, the bending moment is 5000 kN.m. History effects must be considered, the bending moment of 10200 kN.m is added first, then the bending moment is unloaded to 5000 kN.m in later step. Otherwise without taking residual strain into account, the obtained strain in the unloading stage will be much smaller. The tension is 7000 kN and it maintains the same for these two situations. The pipe end is totally fixed under conservative considerations.

The simulation results are shown in Figure 3.2 and Figure 3.3 , the graphs present the longitudinal strain variation under different loading scenario. From the graphs, the longitudinal strain intensification at the pipe section which is close to the buckle arrestor could reach 1.28% when the buckle arrestor is located on the rollers, and it drops to 1.14% when the buckle arrestor is located between the rollers.

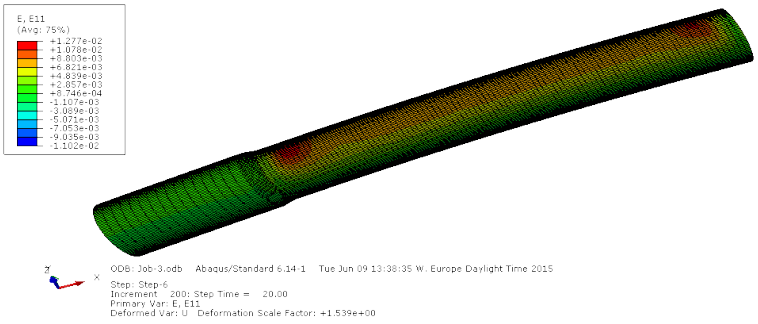

Figure 3.2: Longitudinal Strain - Buckle Arrestor on the Rollers

3.2 Cyclic Loading

Based on the global analysis, cyclic loadings are added on the local model. The loading steps are simplified here, only considering the certain moments when buckle arrestor goes on and drops off the rollers. Because from previous global analysis, the strain variations are much smaller when the buckle arrestor moves on the rollers

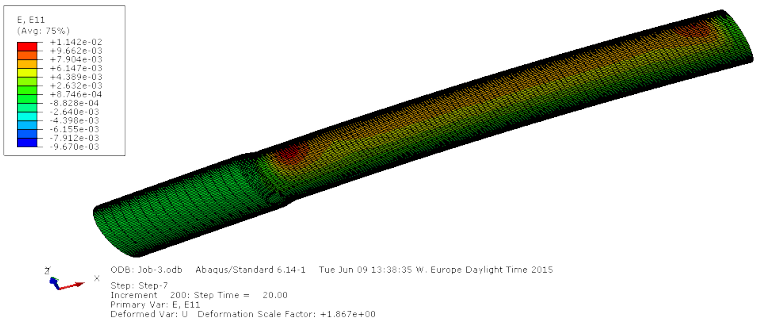

Figure 3.3: Longitudinal Strain - Buckle Arrestor between the Rollers

or the distance between two rollers. These relative small strain variations could be neglected.

The dynamic effect is taken into account, the amplified external bending moments is applied. When buckle arrestor is located on the rollers, the moment is 10200 kN.m. When it is positioned between the rollers, the moment drops to 5000 kN.m. The tension 7000 kN is maintained the same for these two cases, and it is allowed to follow the rotation when bending moment is applied. The loads are applied for three cycles. The relevant strain and stress variations are shown in Figure 3.4 respectively. The longitudinal stress 460 MPa will be used in the later tearing analysis, while the longitudinal stress range 250 MPa will be used in fatigue assessment.

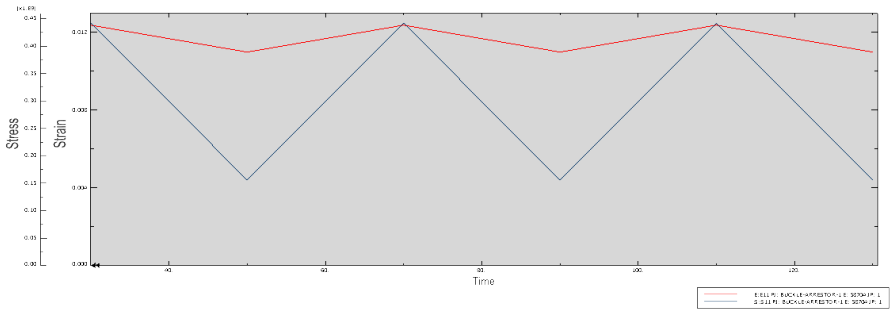

Figure 3.4: Strain & stress under cyclic loading

Figure 3.4 illustrates the perfect plastic behavior of the material as well. During the cyclic loading, once the elastic-perfect plastic material is plastified, no more plastic deformation will happen if the loads are not increased in the next cycle.

Chapter 4

Theory of Engineering Critical Assessment

4.1 Critical Concepts in Fracture Mechanics

4.1.1 J-Integral

The J-integral is based on the energy balance approach.
According to the Griffith Energy Balance Theory, the total energy U of the cracked plate is [5]:

$$U = U_0 + U_a + U_\gamma - F$$

where:
U_0 is the elastic energy of loaded non-flaw plate;
U_a is the change in elastic energy induced by introducing crack in the plate;
U_γ is the change in the elastic surface energy caused by the formation of the crack surface;
F is the energy caused by outside force.

Within some restrictions, the nonlinear elastic behavior of a material could be used to describe its plastic behavior. The main restriction is that no unloading may happen in anywhere of a body since in reality the plastic deformation is irreversible [5].

By definition, the J-Integral is written as:

$$J = -\frac{dU_p}{da}$$

Here the potential energy U_p is defined as:

$$U_p = U_0 + U_a - F$$

According to the Green's theorem, the path independent of the J-Integral expression allows calculation along a contour remote from the crack tip. The contour can be chosen to contain only elastic loads and displacements, thus the elastic- plastic energy release rate can be obtained though it [5].

Because the J-Integral is consider as an elastic-plastic energy release rate, a critical value J_c is defined, which describes the characteristic of a material and predicts the onset of crack growth [5]. The calculated J values can be compared with the J_c, while J must be less than J_c in fracture assessment.

4.1.2 Crack Tip Opening Displacement

The CTOD(Crack Tip Opening Displacement) method was introduced by Wells. The crack tip stress will exceed the yield strength and this leads to plastic deformation. The failure will occur when the plastic strain exceeds the limit state [5].

Wells considered that the stress near the crack tip would always reach the critical value, as a result, the plastic strain in crack tip region controls fracture [5]. A measure of the amount of crack tip plastic strain which in terms of the displacement at the crack flanks, especially near the crack tip. Thus it was expected that at the onset of fracture the Crack Tip Opening Displacement has a critical value for its own material, it could be used as a fracture criterion [5].

In 1966, burdekin and Stone provided an improved basis for the CTOD concept based on the Dugdale strip yield model. The result expression is [5]:

$$\delta_t = \frac{8\sigma_y a}{\pi E} lnsec\left(\frac{\pi\sigma}{2\sigma_y}\right)$$

The equation is only valid for the infinite plate, it is not possible to derive similar equation for particular geometries, thus it is used to compare the fracture resistance of materials.

4.1.3 Stress Intensity Approach

Due to the practical difficulties of energy balance approach, Irwin(1950s) came up with the stress intensity approach. In the linear elastic theory, Irwin illustrated that the stresses near the crack tip could be express in the form [5]:

$$\sigma_{ij} = \frac{K}{\sqrt{2\pi r}} f_{ij}(\theta) + ...$$

where r and θ are the cylindrical polar coordinates of a point with respect to the crack tip.

K is the stress intensity factor which describes the stress magnitude. The general formula of the stress intensity factor is [5]:

$$K = \sigma\sqrt{\pi a} f\left(\frac{a}{w}\right)$$

where $f(\frac{a}{w})$ is a dimensionless parameter which depends on the geometries.

Irwin illustrated that if a crack grows by da, the work done by stress field in front

of the crack when moving through the displacements corresponding to a crack of length$(a + da)$ is formally equal to the change of strain energy(Gda) [5]. Thus the effect of the stress intensity factor is similar to the energy balance approach. Besides the stress intensity factor can be measured experimentally. These are the reasons why stress intensity factor can be widely used in fracture mechanics.

Many standard industry code and some practical papers have given the solution of intensity factor based on different flaw size, shape, specimen geometries, etc. The stress intensity factor can be applicable to stable crack extension, fatigue crack extension, stress corrosions, etc.

4.2 Method of Engineering Critical Assessment

4.2.1 General

The Engineering Critical Assessment is based on the Failure Assessment Diagram which is most widely used methodology for elastic-plastic fracture mechanics of structure components. The original FAD is derived from the strip-yield zone correction, later more accurate FAD is developed from the elastic-plastic J-integral [10]. The FAD approach is versatile, it can be used in brittle fracture under linear elastic conditions and ductile tearing when the loads come to plastic regime. It is also appropriate for the welding part since it takes residual stress into account.

In this case, the defective girth welding which is located near the buckle arrestor may fail when the series plastic loading effects exceed the material resistance. So an appropriate assessment should be performed on its strength capacity. The general steps are:

1. Defining the relevant loads or loading effects.
2. Defining the material fracture resistance.
3. Defining the ultimate crack growth.
4. Accessing the crack growth under the current loading and flaw.

4.2.2 Defining Loads and Stresses

In this case, when the buckle arrestor passes over the stinger, it will go on and drop off the roller-box in several cycles. Thus the girth welding part will suffer from shifty membrane stresses mainly due to global bending moment changing.

When defining the loads and load effects, it contains two phases:
1.Calculating the applied stress/strain without considering defective welds.
2.Assess the loading effects on the defective girth welds.

4.2.3 Nonlinear Stress-Strain Curve

The Ramberg-Osgood equation is defined as follows:

$$\varepsilon = \frac{\sigma}{E}[1 + A_y \left(\frac{\sigma}{\sigma_y}\right)^{n-1}]$$

here σ and ε are the true stress and true strain respectively, the corresponding equations are:

$$\sigma_t = \sigma(1 + \varepsilon)$$

$$\varepsilon_t = \ln(1 + \varepsilon)$$

The parameters A_y and n are defined by fitting specific points, e.g. the ultimate tensile stress and the yield point, defined as the stress at global strain equal to 0.5% [2]. According to these requirements, A_y and n are defined as:

$$n = \frac{\log\left(\frac{\varepsilon_u - \frac{\sigma_u}{E}}{\varepsilon_y - \frac{\sigma_y}{E}}\right)}{\log\left(\frac{\sigma_u}{\sigma_y}\right)}$$

$$A_y = \frac{\varepsilon_y E}{\sigma_y} - 1$$

The material tensile properties should be the weakest material near the flaw [2], this characteristic should maintain the same in the Engineering Critical Assessment. The strength capacity of welds should be at least equal or even higher than the parent material, the objective is to reduce local deformation with any defects.

4.2.4 Defining Fracture Resistance

The fracture toughness is converted to critical stress intensity factor, K_{mat} [2].
When the fracture toughness is obtained from J-integral:

$$K_{mat} = \sqrt{\frac{EJ_{mat}}{1 - \upsilon^2}}$$

Where: υ is the Poisson's ratio.

When fracture toughness is obtained in terms of crack tip opening displacement(CTOD):

$$K_{mat} = \sqrt{\frac{m\sigma_Y \delta_{mat} E}{1 - \upsilon^2}}$$

Where:
δ_{mat} is the fracture toughness in terms of CTOD;
m is obtained by:

$$m = 1.517 * \left(\frac{\sigma_y}{\sigma_u}\right)^{-0.3188}$$

for $0.3 < \frac{\sigma_y}{\sigma_u} < 0.98$, otherwise m is set to 1.5.

4.2.5 Characterize the Flaw Size and Shape

The initial flaw size and the maximum growth should be defined before performing ECA analysis. In this cases, the flaw type is selected as surface elliptical flaw, mainly considering the growth in depth direction, the maximum allowable growth is 1 mm.

4.2.6 Selection of Failure Assessment Diagram

The Failure Assessment Diagram has three alternative levels. The complexity of these levels are increasing due to the required material and stress analysis data [2]. As a result, the accuracy will increase.

In this case, the Option-2 is selected. The failure assessment curve is defined by equation. It needs the mean uni-axial tensile true stress-strain curve at the assessment temperature for stresses up to σ_U and it is suitable for all metals regardless of the stress-strain behavior [2].

To derive the Option-2 curve, detailed stress-strain data are needed especially at strain below 1%. It needs values at $L_r = 0.7, 0.9, 0.98, 1.0, 1.02, 1.1$, then up to $L_{r,max}$ [2].

For $L_r < L_{r,max}$:

$$f(L_r) = \left(\frac{E\varepsilon_{ref}}{L_r \sigma_y} + \frac{L_r^3 \sigma_y}{2E\varepsilon_{ref}} \right)^{-0.5}$$

For $L_r \geq L_{r,max}$:

$$f(L_r) = 0$$

Here the cut-off value $L_{r,max}$ is calculated by:

$$L_{r,max} = \frac{\sigma_y + \sigma_u}{2\sigma_y}$$

4.2.7 Calculation of the Load Ratio L_r

The load ratio The load ratio L_r is determined via:

$$L_r = \frac{\sigma_{ref}}{\sigma_y}$$

σ_{ref} is the reference stress which is calculated according to BS7910-Annex P.

4.2.8 Calculation of the Fracture Ratio K_r

The fracture ratio K_r is determined via:

$$K_r = \frac{K_{I,p} + K_{I,s}}{K_{mat}} + \rho$$

Where:
$K_{I,p}$ is the stress intensity factor at the current crack size due to the primary loads, see BS 7910-Annex M.
$K_{I,s}$ is the stress intensity factor at the current crack size due to the secondary loads, see BS 7910-Annex M.
ρ is used to determine the plasticity interaction effects with combined primary and secondary loading, see BS 7910-Annex R.

The primary loads are the loads that can , if sufficiently high, contribute to fracture failure, fatigue, creep, etc, including external loads, internal pressure [2]. The secondary loads are self-equilibrating loads necessary to satisfy compatibility in structure, thermal stresses and residual stresses are treated as secondary loads which do not contribute plastic collapse [2].

4.3 Ductile Tearing Analysis

4.3.1 Ductile Tearing Mechanism

Ductile crack growth usually follows three stages, micro-void initiation, voids growth near the crack tip, voids coalescence at the tip of a existing crack [10], the Figure 4.2 illustrates the mechanism.

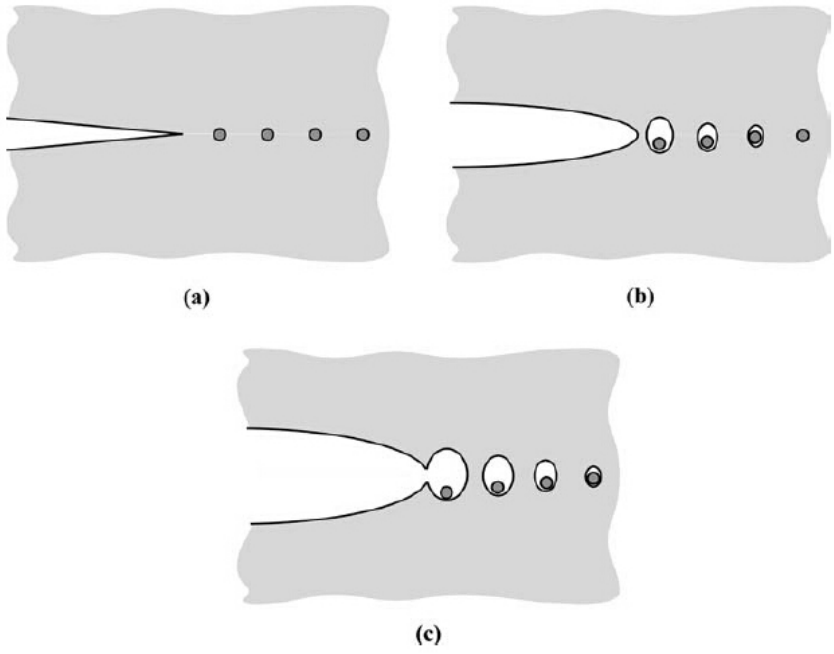

Figure 4.1: Mechanism of Tearing Growth [10]

For a structure which contains flaws, when external loads increase to a certain level, the local stresses and strains near the crack tip are sufficient to nucleate voids. The voids grows gradually and finally become part of main crack, as a result, the crack grows [10].

4.3.2 Ductile Tearing Instability

Ductile crack growth shows stability when the crack driving force change rate is less than or equal to material resistance change rate. The following equations define the tearing modulus [10].

$$T_{app} = \frac{E}{\sigma^2}\left(\frac{dJ}{da}\right)_{\Delta_T}$$

and

$$T_R = \frac{E}{\sigma^2}\frac{dJ_R}{da}$$

where ΔT is the remote displacement:

$$\Delta T = \Delta + C_M P$$

where C_M is the system compliance, as shown in Figure 4.2. C_M influences structure instability. $C_M = \infty$ represents dead loading which means unstable; $C_M = 0$ means the other extreme displacement control, the structure is more stable [10]. The crack is unstable when $T_{app} > T_R$.

The driving force change rate at a fixed remote displacement is:

$$\left(\frac{dJ}{da}\right)_{\Delta T} = \left(\frac{\partial J}{\partial a}\right)_P - \left(\frac{\partial J}{\partial P}\right)_a \left(\frac{\partial \Delta}{\partial a}\right)_P [C_M + \left(\frac{\partial \Delta}{\partial P}\right)_a]^{-1}$$

The fracture resistance change rate is:

$$J_R = J_R(a - a_0)$$

For the assessment of tearing stability, two alternative methods could be used, crack driving force diagram and stability assessment diagram. Crack driving force diagram plots J and J_R vs. crack length, while stability assessment diagram plots tearing modulus vs J.

Figure 4.3 illustrates the mechanism of crack driving force diagram for both load control and displacement control. In this graph, for load control, crack is unstable at P_3, while for displacement control, at Δ_3 it is stable.

Figure 4.4 is a stability assessment diagram. It plot T_{app} and T_R against J and J_R respectively. Crack becomes unstable when the $T_{app} - J$ curve crosses the $T_R - J_R$ curve.

4.3.3 Ductile Tearing with Failure Assessment Diagram

Ductile tearing analysis can be combined with Failure Assessment Diagram. This method is essentially similar to the crack driving force diagram and stability assessment diagram, it plots crack driving force and material fracture resistance in terms

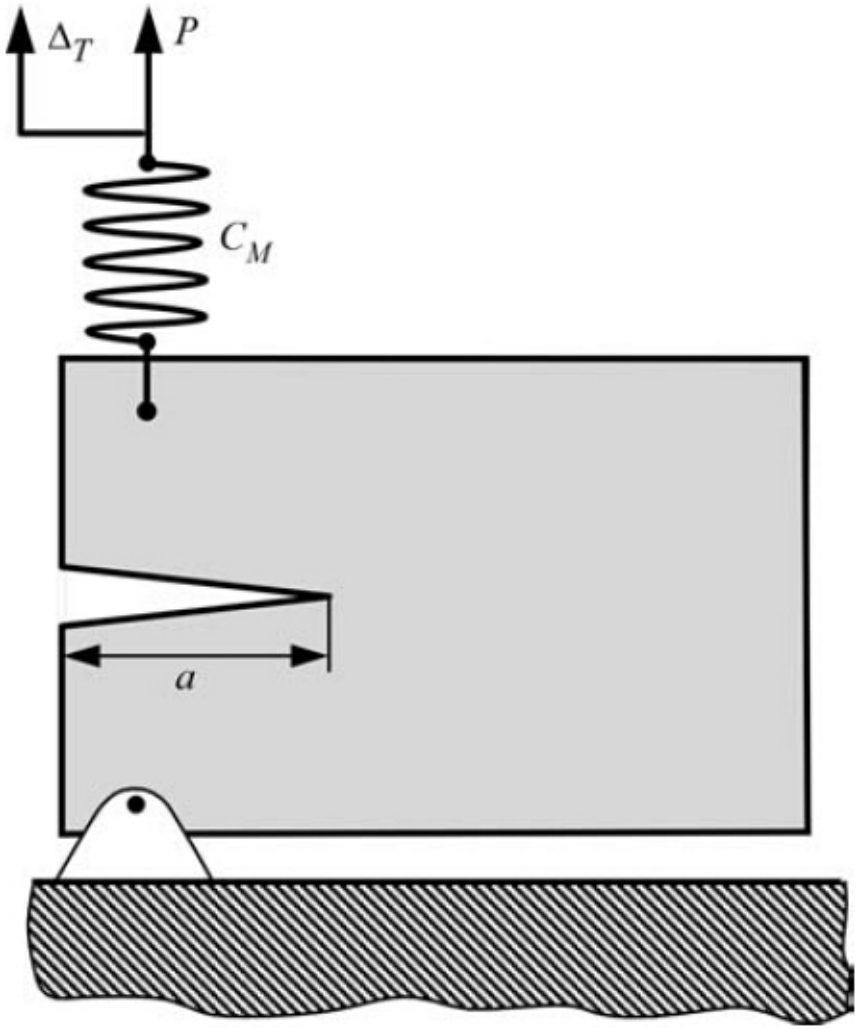

Figure 4.2: A cracked structure with finite compliance [10]

of K_r and L_r [10].

In this case, the option 2 is selected to assess the ductile tearing behavior of defective girth welds. Several amounts of tearing crack growth are postulated, the fracture ratio K_r and the load ratio L_r are calculated based on the updated flaw size which equals to the current flaw size plus the increased crack growth [2], both flaw size and fracture toughness should be updated as crack growth. The maximum allowable crack growth is 1mm.

In each cycle, all pairs (L_r,K_r) are functions of updated flaw size. The initial flaw size shall be evaluated at initial fracture toughness $K_{0.2mm}$ [2], followed by flaw size based on amounts of tearing growth at a fixed load.

The calculated pairs (L_r,K_r) are plotted on the FAD diagram. If the locus line is completely located outside the FAD, the flaw is unacceptable; if the locus line crosses the boundary of FAD, some ductile tearing could occur. Figure 4.5 shows

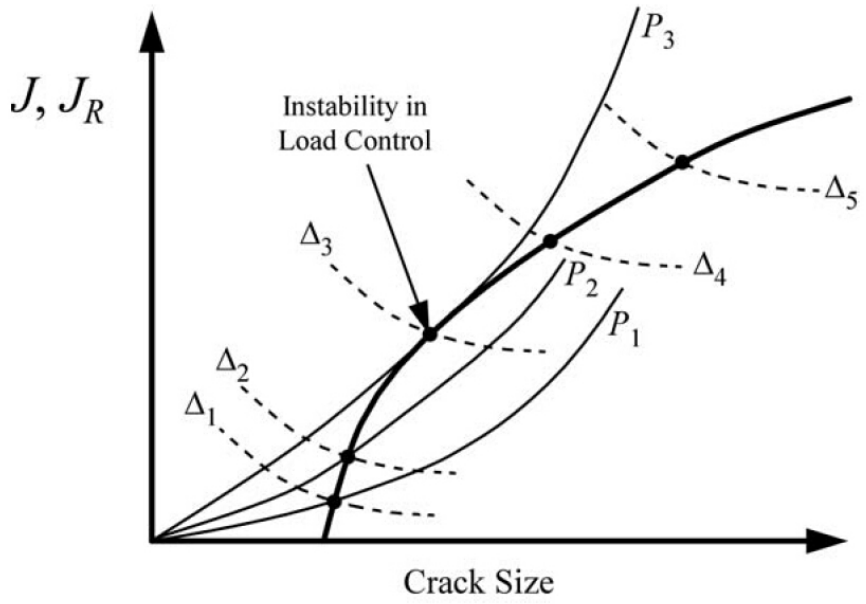

Figure 4.3: J, J_R vs crack size [10]

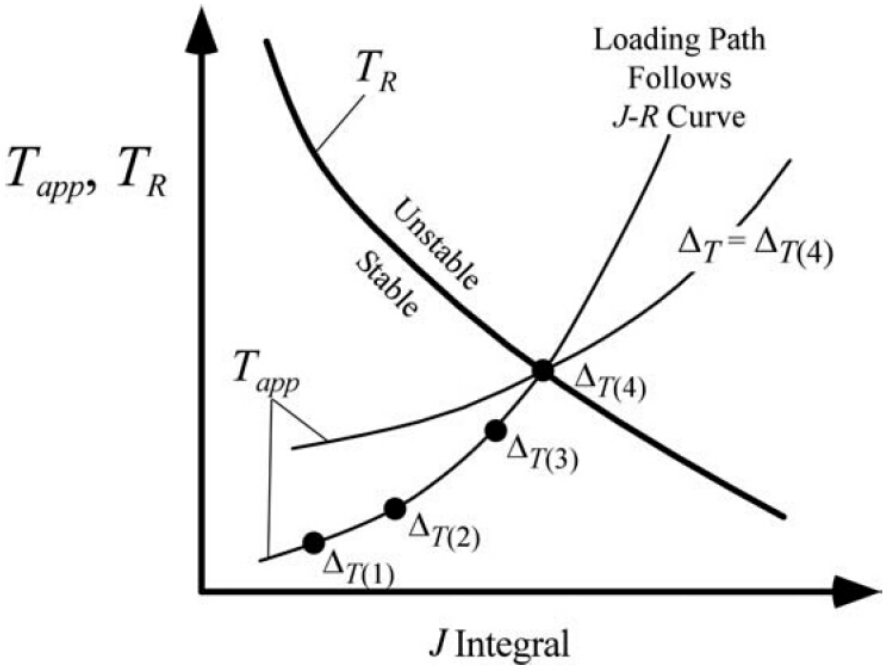

Figure 4.4: T, T_R vs J [10]

three possible results of ductile tearing assessment.

The whole analysis is based on the loading control. However the ductile tearing assessment would be conservative if the loading control are nearly close to displacement control [10].

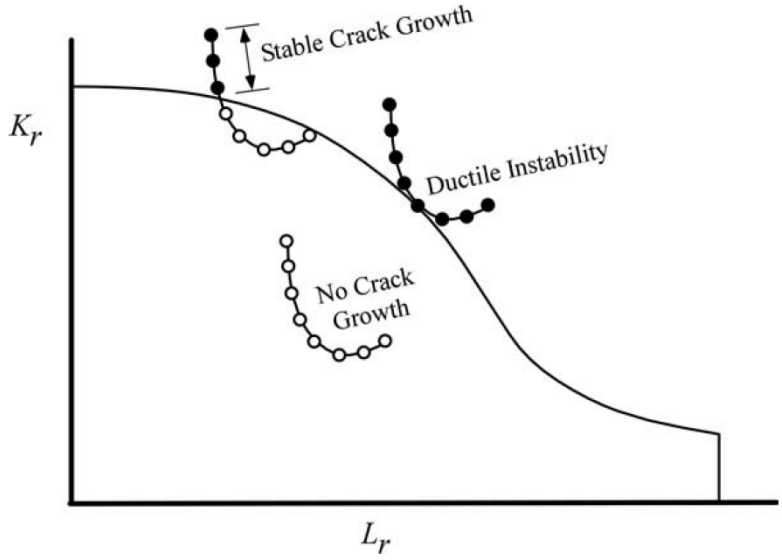

Figure 4.5: Ductile Tearing with FAD [10]

4.4 Fatigue Crack Growth Assessment

4.4.1 Fatigue Analysis

To analysis the crack growth under fatigue loading, the general method is to estimate the fatigue life by integrating the crack growth law. It is allowable to use the accurate cyclic stress intensity factor expressions and specific fatigue crack growth data [2].

In the fatigue fracture assessment, conservative estimation of the fatigue parameters are needed. It is assumed that an idealized flaw as a sharp tipped crack that propagates under the crack growth rate law, da/dN, and the range of stress intensity factor, ΔK [2]. The general relationship between da/dN and ΔK is simplified to a sigmoid curve in a $\log(da/dN)$ versus $\log(\Delta K)$ plot [2]. As shown in Figure 4.6.

For the corresponding equation, the Paris law is as follows:

$$\frac{da}{dN} = A * (\Delta K)^m$$

A and m are constants that depend on material and applied conditions, including environment and cyclic frequency;

For $\Delta K < \Delta K_0$, da/dN is assumed to be 0.

The stress intensity factor range, ΔK, is a function of geometry, stress range and instantaneous crack size, and it is calculated from the following equation:

$$\Delta K = Y(\Delta\sigma) * \sqrt{\pi a}$$

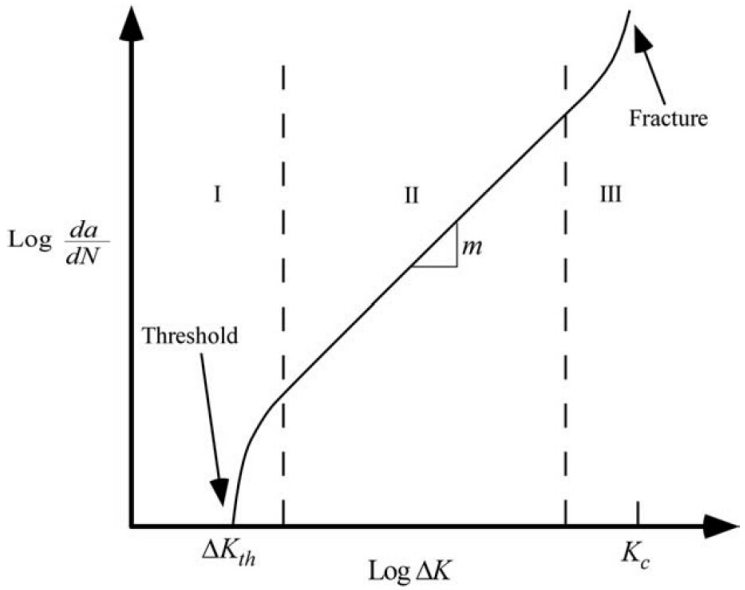

Figure 4.6: Paris Law [2]

The general equation of $Y(\Delta\sigma)$ is given in BS 7910 Annex M.

4.4.2 General procedure of assessment

The crack growth relationship and relevant value of ΔK_0 is determined from the Table 4.4.2. For elliptical flaws, it is usually assumed that the relationship of crack growth in both depth and length directions is the same.

Table 4.1: Recommended fatigue crack growth threshold-Δk_0

Material	Environment	ΔK_0 $N/mm^{1.5}$
Steels,including austenitic	Air or other nonaggressive environments up to 100 °C	63
Steels,excluding austenitic	Marine with cathodic protection, up to 20 °C	63
Steels,including austenitic	Marine,unprotected	0
Aluminium alloys	Air or other nonaggressive environments up to 20 °C	21

In this case, the relevant stress range of series cyclic loading are obtained from previous local FEM analysis, including membrane stress range and bending stress range. It is always necessary to estimate the worst cases.

For the assumed initial flaw, the relevant stress intensity factor range ΔK corresponding to the applied stress range should be estimated. The solutions of the ΔK

is calculated according to BS 7910 Annex-M. For the partial-thickness or embedded flaws, ΔK should be calculated at the end of both minor and major axis of the idealized elliptical flaw[BS 7910].

For the crack growth, Δa is estimated in one cycle from the calculated ΔK using the Paris law which is determined previously. As a result, in the first cycle, the initial flaw a is increased by Δa. Similarly, the growth of Δc in one cycle is calculated in the same way, while in the end, the length of flaw 2c is increased by $2\Delta c$.

For the next cycle, the initial flaw a equals to $a + \Delta a$, c equals to $c + \Delta c$, reproduce the previous procedure based on the new flaw dimensions and corresponding stress range.

In the end, under the cycle ranges, the accumulated crack growth is calculated. If it does not exceed the limit crack growth, the flaw is regarded as acceptable, otherwise, the initial flaw is not acceptable.

Chapter 5

Crack Growth Estimation

5.1 Description of Simplified Method

For the tearing crack growth, when the buckle arrestor is positioned on the roller-box, due to the strain intensification at the top of girth welding part, the crack is opened and tearing growth happens. While when it is located between the roller-boxes, the strain reduces and the crack is partially closed.

In the fatigue crack growth, at the certain moments when the buckle arrestor goes on and drops off the roller-boxes, the stress variation is quite high and fast, it can be regarded as high cyclic fatigue. During the stages when the buckle arrestor passes over the roller-boxes and the distance between two roller-boxes, the dynamic effects which introduced by the ship motions and waves are considered. These stress variations can be simplified as sinusoidal format, the cycles are sufficient while their amplitudes are relatively low.

In a conservative way, the total crack growth Δa_{tot} is determined by the superpositions of the tearing crack growth and the fatigue crack growth:

$$\Delta a_{tot} = \Delta a_f + \Delta a_t$$

5.2 Ductile Tearing Growth

5.2.1 General Calculation Procedure

According to the previous analyses, the girth welding part will be subjected to cyclic loading when the buckle arrestor passes over the stinger, especially the moment when buckle arrestor goes on the roller-boxes, the local strain at the top of girth welding part increases a lot. To calculate the tearing crack growth under these cyclic loading situation, there are three assumptions based on the fracture resistance curve which lead to different results.

The ductile tearing growth is calculated by the combination of Failure Assessment Diagram which specified in BS 7910. The whole calculation procedures are programmed in Python.

Surface elliptical flaw is taken into account here, only depth growth is considered. The reason is that:

$$\frac{a}{t} = \frac{0.002}{0.039} \approx 0.05$$

$$\frac{c}{C} = \frac{0.025}{3.86} \approx 0.009$$

where t is the pipe wall thickness, C is the pipe circumference.
The ratio in the depth direction is relatively high, therefore the crack growth mainly happens in the depth direction.

At the beginning, according to the initial flaw size $a \times c$, the K_r and the L_r are calculated respectively. The assess point (K_r,L_r) locates outside the boundary of the Failure Assessment Diagram which means that the current flaw is unstable. Then the a is increased by Δa (0.01 mm), based on the updated flaw size, the new K_r and L_r are calculated, the access point is compared with the Failure Assessment Diagram again. Subsequently, the calculation procedure is reproduced cycle by cycle until the assess point is located at the boundary of the Failure Assessment Diagram, finally the crack is stable. The total crack growth is equal to the sum of all Δa.

In the second cycle, initially when calculating the K_r, the stress intensity factor K_I is based on the flaw size which is updated at the end of first cycle.

While for the K_{mat}:

$$K_{mat} = \sqrt{\frac{m\sigma_Y \delta_{mat} E}{1 - \upsilon^2}}$$

The δ_{mat} is the material fracture resistance in terms of the CTOD, and the CTOD is expressed as:

$$CTOD = CTOD_{initial} + C_1(\Delta a)^{C_2}$$

For the determination of the $CTOD$, three assumptions are made, which are Material Memory R Curve, History Independent R Curve, History Dependent R Curve. They are calculated separately.

The L_r is also based on the previous end reached flaw size. The assess point (K_r,L_r) is compared with the FAD, if it is outside the diagram, the a is increased by Δa. The similar calculations are reproduced continuously until the assess point locates at the boundary of the FAD.

The subsequent assessment procedures maintain the same. 20 cycles are taken into account and the crack growth of each cycle are added up together. If the total crack

growth of 20 cycles is less than the limit state 1mm, the initial flaw can be regarded as safe, otherwise it is dangerous.

5.2.2 Assumption 1 - History Independent R Curve

The history independent R curve neglects the history loading effects. Each cycle is relatively independent which means that the previous end reached CTOD has no influence on the initial CTOD of the next cycle, as shown in the Figure 5.1.

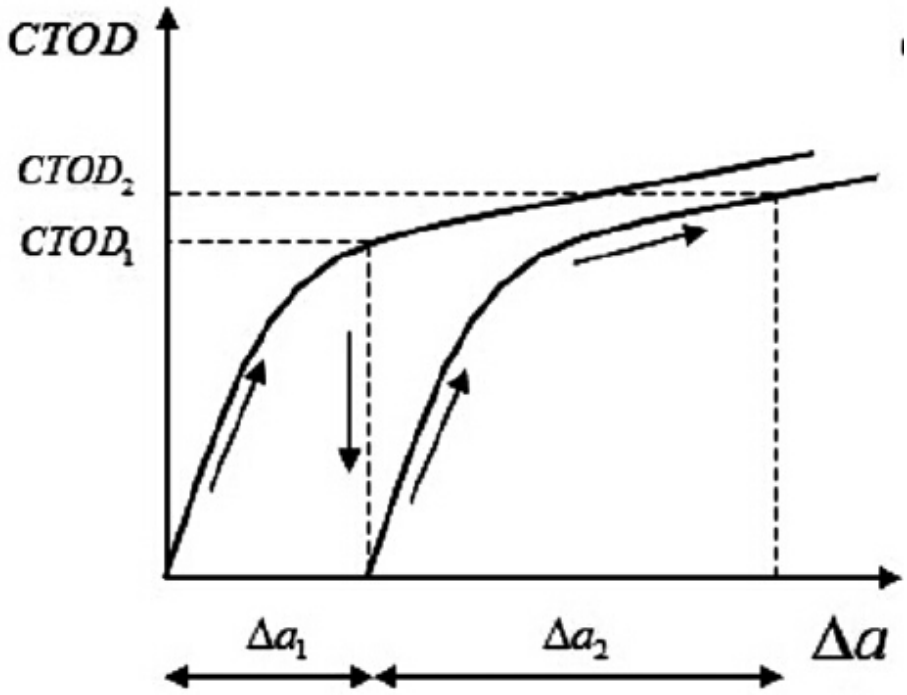

Figure 5.1: History Independent R Curve [4]

The CTOD-R curve just shifts to the right side based on the previous crack growth, the initial fracture resistance maintains the same level for each cycle. 20 cycles are considered here. The calculations are carried out on two different flaw sizes, as presented in Table 5.1 and Table 5.2.

In the tearing crack growth, the History Independent R Curve is quite conservative, the crack grows in each cycle. When the initial flaw depth is 2 mm, after 20 cycles, the crack growth is 0.7 mm. While when the initial flaw depth becomes 2.5 mm, the total crack growth nearly reach the maximum allowable growth, 1 mm. So if there are much more cycles, there will be more crack growth. And if the initial flaw size is larger, it is easier to reach the limit state.

However this assumption is not suitable for the real situation since it totally neglects the loading history effects. It is similar to this situation. A group of specimens, except the initial flaw size is different, other conditions are all the same. Tearing tests are carried out on these specimens, under the same loading, definitely the specimen

Table 5.1: Tearing Growth - Flaw 2×25 mm (History Independent R Curve)

Cycles	Flaw Depth (mm)	Depth Growth (mm)
1	2	0.029
2	2.029	0.029
3	2.058	0.03
4	2.088	0.03
5	2.118	0.031
6	2.149	0.032
7	2.181	0.032
8	2.213	0.033
9	2.246	0.034
10	2.28	0.034
11	2.314	0.035
12	2.349	0.036
13	2.385	0.037
14	2.422	0.037
15	2.459	0.038
16	2.497	0.039
17	2.536	0.04
18	2.576	0.04
19	2.616	0.041
20	2.657	0.042

with bigger initial flaw size will have larger crack growth.

In reality, plastic deformation is generated around the crack tip during tearing growth. Then under partial unloading, the crack closes a bit, there will be reverse plastic region in front of the crack tip. The reverse plastic region could reduce the fracture resistance and lower the material yield property. However the size of the region is small and limited, it depends on the unloading level. Even if the external loads are total released and reverse loading is added the other plastic deformation part which around the reverse plastic region can not go back to the initial state totally. So the fracture resistance reached at the end of previous cycle can not totally return to original state.

5.2.3 Assumption 2 - Material Memory R Curve

The Material memory R curve is based on the history loading effects. The fracture resistance does not shift to a new origin for the next cycle. The crack driving force obtained at the end of previous cycle must be reached at the beginning of the next cycle, then the crack is allowed to grow under larger loading. However the material must be elastic - perfect plastic in this assumption. The mechanism is shown in Figure 5.2

Table 5.2: Tearing Growth - Flaw 2.5 × 25 mm (History Independent R Curve)

Cycles	Flaw Depth (mm)	Depth Growth (mm)
1	2.5	0.039
2	2.539	0.04
3	2.579	0.041
4	2.62	0.041
5	2.661	0.042
6	2.703	0.043
7	2.746	0.044
8	2.79	0.045
9	2.835	0.046
10	2.881	0.047
11	2.928	0.048
12	2.976	0.049
13	3.025	0.05
14	3.075	0.051
15	3.126	0.052
16	3.178	0.053
17	3.231	0.055
18	3.286	0.056
19	3.342	0.057
20	3.399	0.058

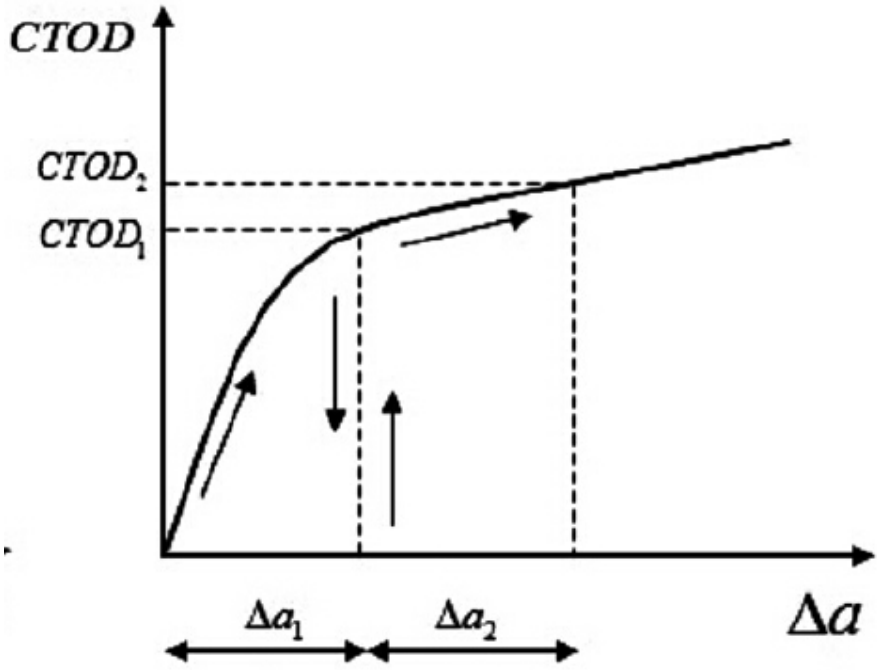

Figure 5.2: Material Memory R Curve [4]

From the graph, it is clear to see that during cyclic loading, the previous end reached CTOD remains unchanged; for the next cycle, only when larger crack driving force is applied, further tearing growth will happen. The calculation results are shown in Table 5.3. In the Material Memory R Curve, the assumption of perfect elastic-

Table 5.3: Tearing Growth - Flaw 2 × 25 mm (Material Memory R Curve)

Cycles	Flaw Depth (mm)	Depth Growth (mm)
1	2	0.029

plastic material property is made, and there is no change in the material property under the loading history. In the first cycle, the judge point is located outside the Failure Assessment Diagram which means the initial flaw is unstable, then the tearing growth happens until the crack is stable when the assess point is located at the boundary of Failure Assessment Diagram, as plotted in Figure 5.3, the red line is the local assessment line.

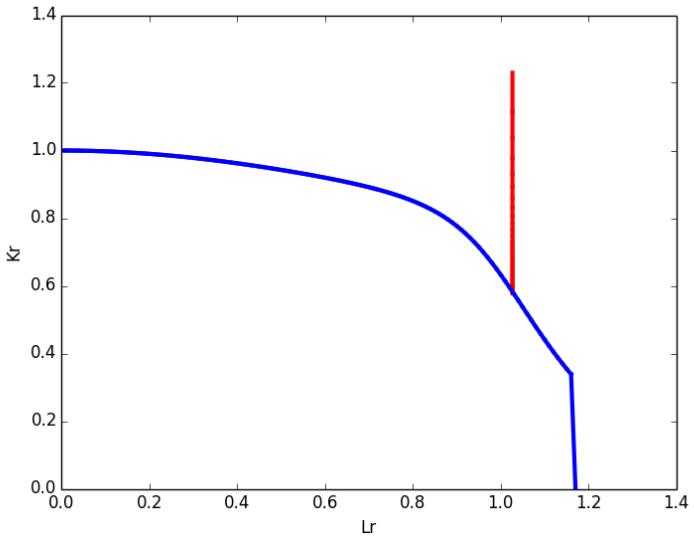

Figure 5.3: Failure Assess Diagram-One Cycle

Under this assumption, the fracture resistance reached at the end of first cycle maintains the same level for the beginning of second cycle. So in these two certain moments, the flaw size, the fracture resistance, the external loads and material property are all the same. As a result, the calculated K_r and L_r are equal, the judge point still locates at the boundary of Failure Assessment Diagram, crack is stable. Subsequently, in the following cycles, no any further tearing crack growth appear, unless the external stress increases.

In reality, the perfect elastic-plastic material does not exist. Under the cyclic loading, especially when large plastic deformation generates, the material property and

fracture property will be changed locally. Especially when the load ratio is negative (reverse loading), the reduction of the fracture resistance becomes more pronounced [9]. Thus in the later cycles, tearing crack growth may happen.

5.2.4 Assumption 3 - History Dependent R Curve

It is a common sense that plastic deformation will not only change the yield and flow property, but also affect local fracture mechanisms, the initial fracture resistance and fatigue properties [8]. The Material Memory R Curve can not present the pre-strain history effect on the fracture resistance accurately. Because it assumes that the material is elastic-perfect plastic, and no any change of the material fracture property under the plastic loading. While the History Independent R Curve totally neglects the plastic deformation history. The History Dependent R Curve, as shown in Figure 5.4, should be evaluated properly.

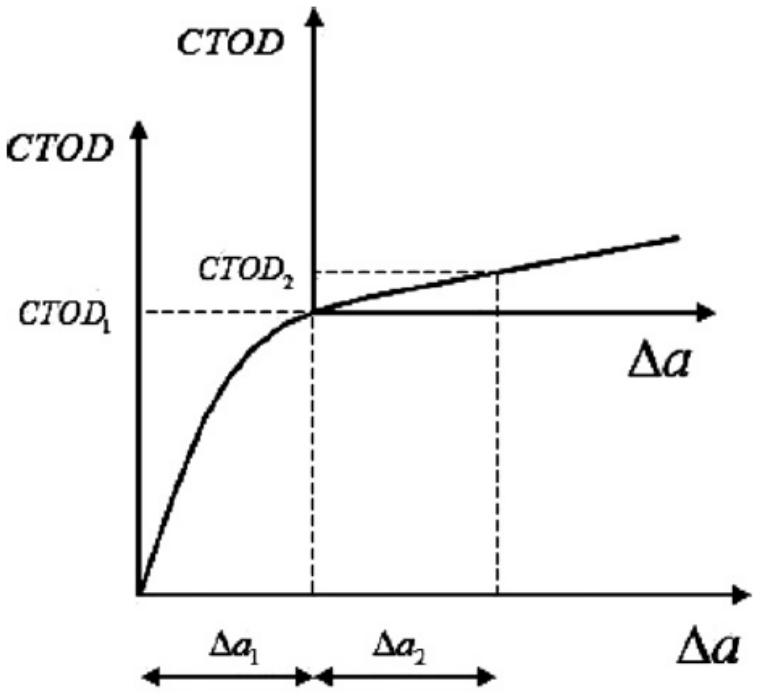

Figure 5.4: History Dependent R Curve [8]

Under the cyclic plastic loading history, the initial fracture resistance of the later cycle will not drop to original state, and it will also not remain the same level as previous cycle reached, the value will between them. It mainly depends on the unloading level or even reverse loading.

In this case, when the buckle arrestor is positioned on the roller-boxes, the strain at girth welding part reaches around 1.28%; when it is located between the roller-boxes, the strain drop to 1.14%. Here since the reduction of fracture resistance is hard to estimate, it is assumed that the initial fracture resistance drop to 50% and

75% of previous end reached CTOD respectively. The relevant results are shown in the following tables.

Table 5.4: Tearing Growth - Flaw 2 × 25 mm (History Dependent R Curve)

Cycles	Flaw Depth (mm)	Growth (mm)
1	2	0.029
2	2.029	0.014
3	2.043	0.014
4	2.057	0.015
5	2.072	0.014
6	2.086	0.015
7	2.101	0.015
8	2.116	0.015
9	2.131	0.015
10	2.146	0.015
11	2.161	0.015
12	2.176	0.016
13	2.192	0.015
14	2.207	0.016
15	2.223	0.016
16	2.239	0.016
17	2.255	0.016
18	2.271	0.016
19	2.287	0.016
20	2.303	0.017

As reflected from the calculation results, fewer reduction of the previous end reached fracture resistance, less crack growth happens in the subsequent cycles. The reduction of the fracture resistance may depend on the unloading level or even the reverse loading, the strength of basic material, etc.

Under this assumption, the tearing crack growth happens continuously when the buckle arrestor passes over the rollers, besides the crack growth of each cycle gradually increases. In real installation, if some emergency happens, the pipe is pulled back, the buckle arrestor experiences more cycles. In the end, the crack growth may exceed the limit state which will be dangerous.

5.3 Fatigue Crack Growth

According to the Paris-Erdogan Law which is illustrated in the previous chapter and the assumption of these loading ranges, the fatigue crack growth are carried out. According to the instructions in the BS 7910, the selected fatigue crack growth laws

Table 5.5: Tearing Growth - Flaw 2×25 mm (History Dependent R Curve-75%)

Cycles	Flaw Depth (mm)	Growth (mm)
1	2	0.029
2	2.029	0.005
3	2.034	0.005
4	2.039	0.005
5	2.044	0.005
6	2.049	0.006
7	2.055	0.006
8	2.061	0.006
9	2.067	0.006
10	2.073	0.006
11	2.079	0.006
12	2.085	0.006
13	2.091	0.006
14	2.097	0.006
15	2.103	0.006
16	2.109	0.006
17	2.115	0.006
18	2.121	0.006
19	2.127	0.006
20	2.133	0.006

are presented in Table 5.6. The calculation procedures are achieved in the Python. The Table 5.7 presents the results.

Table 5.6: Fatigue Crack Growth -Constants

Stage	ΔK N/mm$^{3/2}$	m	A
A	63	5.1	2.1×10^{-17}
B	144	2.88	1.29×10^{-12}

Table 5.7: Fatigue Crack Growth - Flaw 2×25 mm

Type	Cycles	$\Delta\sigma$[MPa]	Initial Flaw $a \times c$[mm]	Final Flaw $a \times c$[mm]
1	20	250	2×25	2.009×25.0064
2	400	50	2×25	2.002×25.001

It is obvious that when the buckle arrestor passes over the whole stinger, even if all possible fatigue loading are taken into account, the contributions of fatigue crack

growth in both depth direction and length are relatively small, this is mainly due to the limited cycles. Thus the fatigue crack growth almost can be neglected in this case.

Chapter 6

Literature Review and Results Analysis

6.1 Previous FEM Research

The effects of pre-strain history on the fracture resistance have been conducted in some FEM researches. P.A. Eikrem and Z.L.Zhang have carried out the relevant numerical research to study how a reeling induced pre-strain history affects the fracture resistance of an existing crack [8].

In their study, a complete Gurson model was developed for the ductile tearing analysis, by combining the Gurson-Tvergaard-Needleman model with the Thomason's plastic limit load model.

The yield function of the Gurson-Tvergaard-Needleman model [8]:

$$\phi(q, \sigma_f, f^*, \sigma_m) = \frac{q^2}{\sigma_f^2} + 2q_1 f^* cosh(\frac{3q_2\sigma_m}{2\sigma_f}) - 1 - (q_1 f^*)^2$$

Where:
f^* is the void volume fraction;
σ_m is the mean stress;
q is the von Mises stress;
σ_f is the flow stress;
q_1 and q_2 are parameters introduced by Tvergaard to modify the original Gurson model.

The void volume fraction is defined as:
For $f \leq f_c$,

$$f^* = f$$

For $f_c \leq f \leq f_f$,

$$f^* = f_c + (f - f_c)\frac{f_u - f_c}{f_f - f_c}$$

For $f_f \leq f$,

$$f^* = f_u$$

The Thomason's plastic limit load criterion [8] is used to determine the critical volume fraction f_c. Under this modification, the f_c is not a input parameter anymore, it is the result of plastic deformation.

$$\frac{\sigma_1}{\sigma_f} = \frac{0.3}{r/(R-r)} + 0.6$$

Where:
σ_1 is the maximum principle stress;
r and R are current average void radius and intervoid distance which can be calculated from the current principle strains.

2D single edge notched tension(SENT) specimens were used in Abaqus modeling. The void growth is only allowed under tensile deformation and during compression it is suppressed, no element is allowed to fail completely during plastic deformation. Using nominal strain which is defined by the ratio of applied displacement divided by the initial length as external loading parameters [8]. Both symmetrical and non-symmetrical pre-strain cycles are investigated, as presented in Figure 6.1, Figure 6.2, Figure 6.3, and Figure 6.4.

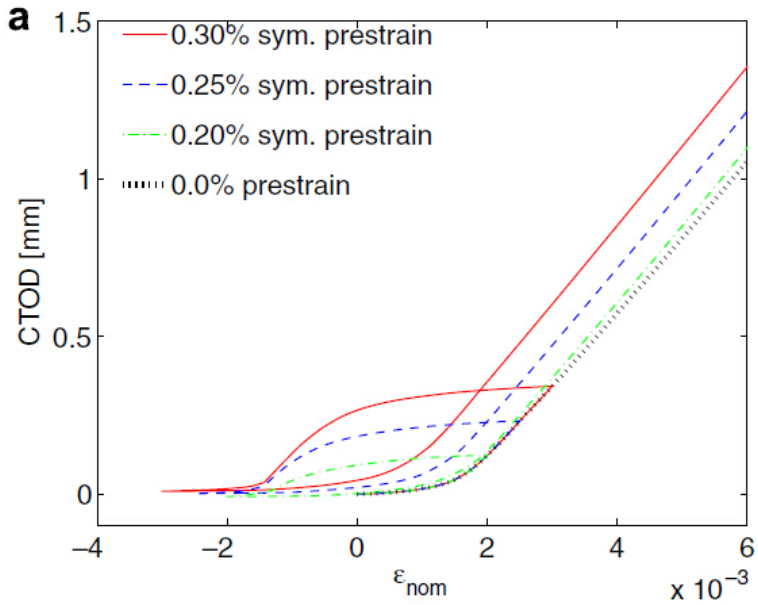

Figure 6.1: CTOD vs Different Symmetrical Pre-strain Cycles [8]

From the upper figures, for the symmetrical pre-strain loading, a pre-strain up to 0.2% could already reduce both the initial fracture toughness and crack growth resistance for the following cycles. When pre-strain reaches 0.3%, the initial fracture resistance is nearly equal to zero for the next loading step, this means that the crack growth starts at the beginning of the next tensile loading step.

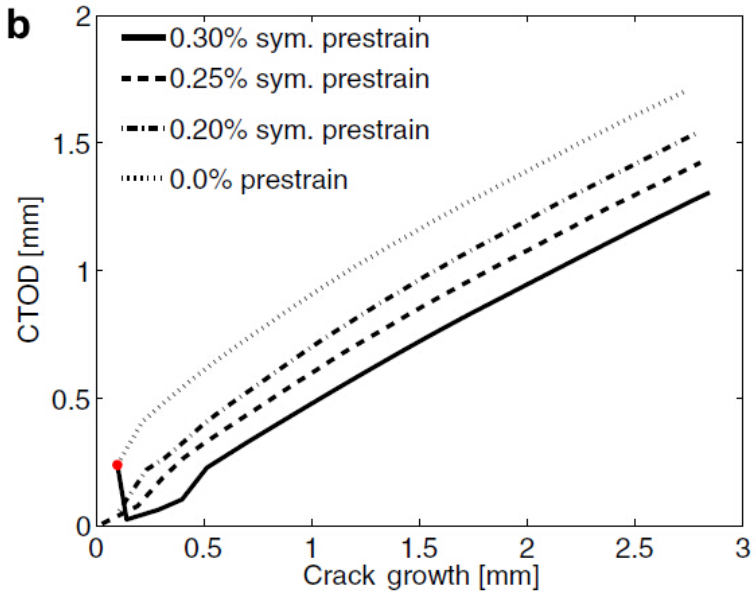

Figure 6.2: Effects of Different Symmetrical Pre-strain on the Fracture Resistance [8]

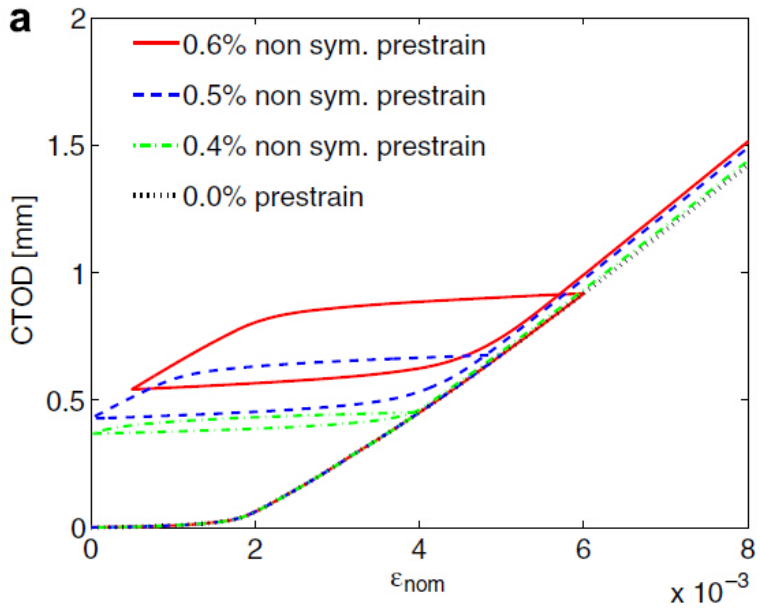

Figure 6.3: CTOD vs Different Non-symmetrical Pre-strain Cycles [8]

As reflected from the figures, in the non-symmetrical pre-strain cases, the crack growth happened under the pre-strain loading. The CTOD reached at the end of pre-tension will be reduced once the compressive loading is added. Thus in the next loading stage, the crack growth will start at a CTOD which is higher than the initial CTOD of the monotonic loading, but lower than the pre-tension end CTOD.

The pre-strain loading history could influence the initial fracture resistance of the

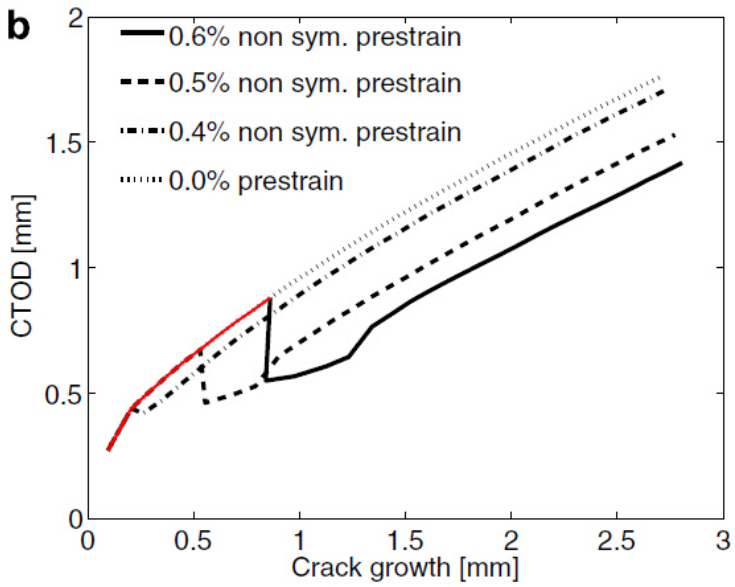

Figure 6.4: Effects of Different Non-symmetrical Pre-strain on the Fracture Resistance [8]

next loading stage, especially when high compressive loading is added in the previous cycle. While as mentioned in the study, the model neglects the change in the material property and stress redistribution, only small pre-strain amplitude and single pre-strain cycle are considered. In reality, during installation, more cycles exist and strain amplitude is larger, the behavior of material fracture resistance, failure mechanisms and failure modes need to be investigated through systematic experiments [8].

6.2 Similar Experiments Study

6.2.1 Case One

Experiment Overview

Tenaris, CSM and Saipem launched a series of experiments aimed at evaluating the in-service flaw acceptabilities of girth welded seamless pipes produced by Tenaris for offshore applications [7]. The objectives of the research are:
-Evaluate the tolerability of defective girth weld;
-Update the experiment data of girth weld tolerance under in-service conditions;
-Evaluate the applicability of ECA tools.

Experiment scenario

The applied strain are under full scale testing:
-High internal pressure – simulate real operation situation;
-One high plastic tensile strain ε_1 – accidental load;
-Cyclic limited strain range $\Delta\varepsilon$ – thermal-induced loading at shut down during

service life.

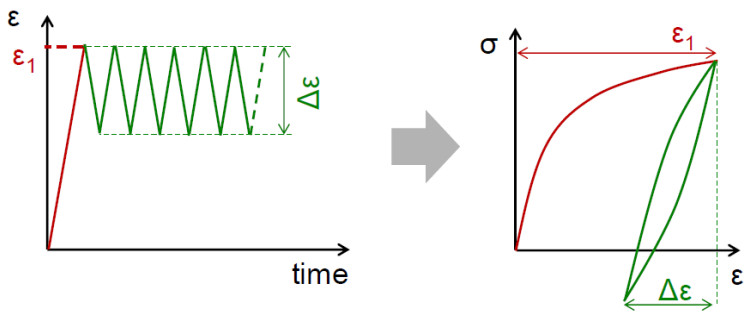

Figure 6.5: Applied Strain Mechanism [7]

Full Scale Testing

The pipe geometry, loading scenarios, notches configurations of the four groups test are present in Table 6.1

Results Summary and Analysis

The full scale test results are summarized in Figure 6.6.

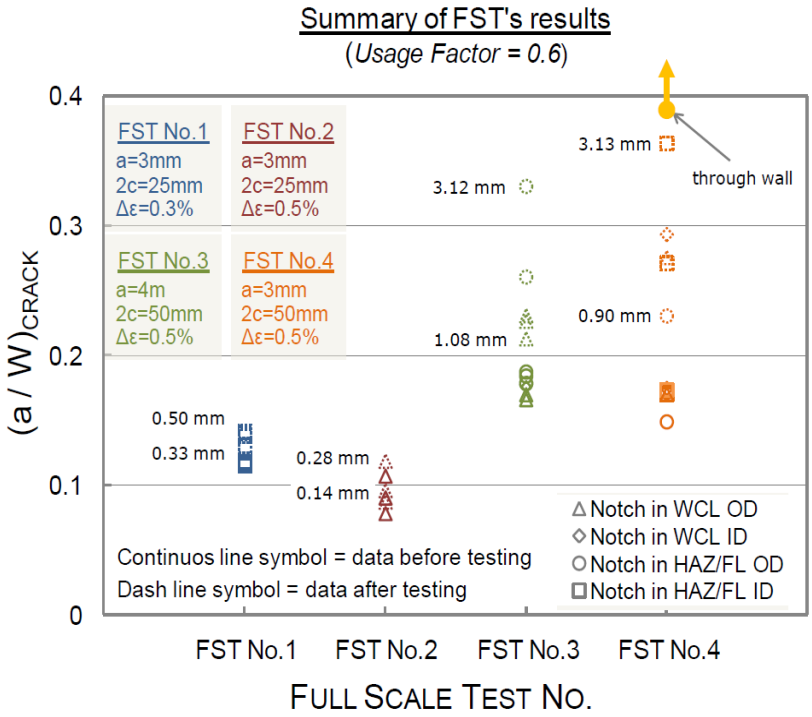

Figure 6.6: Full Scale Test Results [7]

For the first group test, according to the Figure 6.5, at the beginning, the total strain

Table 6.1: Characteristics of Full Scale Testing [7]

No.1	No.2	No.3	No.4
Outside Diameter (mm)			
296.5	296.5	296.5	273
Wall Thickness (mm)			
21.2	21.2	21.2	15.9
Internal Pressure-Hoop Stress			
60% SMYS	60% SMYS	60% SMYS	60% SMYS
Total Axial Strain (%)			
1.0	1.0	1.0	1.0
Strain Range (%)			
0.3	0.5	0.5	0.5
Number of Cycles			
200	200	200	till failure
Flaw size (mm)			
3 × 25	3 × 25	3 × 25	3 ×25
Weld Characteristic			
1 flaw per weld, HAZ/FL, ID surface	1 flaw per weld, WCL, OD surface	2 flaws per weld, 1 in WCL, 1 in HAZ/FL, OD surface	1st flaw HAZ/FL, 2nd flaw HAZ/FL weld cap removal, 3rd flaw WCL weld cap removal

increase to 1%, then the cyclic loading range 0.3% is added. When performing the ECA, in the first cycle, the total strain is used to calculated the tearing growth; in the subsequent cycles, the strain range is used in fatigue growth. The calculations are based on the BS 7910, the tearing growth is 0.27 mm, the fatigue growth is 0.36 mm, so the total crack growth is 0.63 mm [7]. Compared with the experiments results, the average total growth is 0.43 mm, the maximum total growth is 0.50 mm. Though the ECA results is slightly conservative, it is applicable to this kind of loading regime.

While for the other group tests, the strain range is 0.5%, it involves quite large plastic deformation, higher compressive loading is added, no any well-defined and common recognized assessment procedure exist at present [7]. The experiments results could be used for future relevant research study.

6.2.2 Case Two

Experiment Overview

P.K.Singh, V.R.Ranganath, etc. launched a series of experiments to study the effect of cyclic loading on the elastic-plastic fracture resistance of the primary heat transport system piping material of pressurized heavy water reactors [9].

The cyclic J-R curve tests are carried out on CT specimen, quasi-static loading conditions are conducted. In the first cycle, the pre-cracked specimen is loaded to the pre-determined load line displacement(LLD) and then unloaded to the point which is based on the specified load ratio [9]. In the next cycle, the loading is added to an increased LLD, then it is unloaded to such a point to maintain the load ratio. The loading procedure is repeated in sufficient cycles to determine the J-R curve. The loading scheme is shown in Figure 6.7.

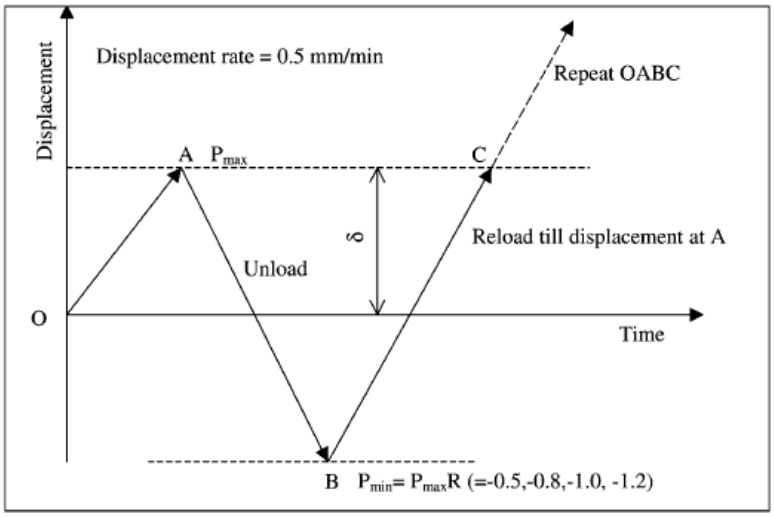

Figure 6.7: Cyclic Loading Scheme [9]

Experiment Results

Systematic experiments are carried out to study the effect of load ratio and the effect of incremental plastic displacement. The effects of load ratio on the material fracture resistance are shown in Figure 6.8 and Figure 6.9.

From the figures, it is observed that under the specific plastic displacement increment, the J-R curve at load ratios of 0.8 and 0 are almost equal; while when the load ratio becomes negative, especially when the load ratio approaches -1, the material fracture resistance drops a lot. This means that under cyclic loading, the increased compressive load could decrease the material strength capacity which in terms of fracture resistance.

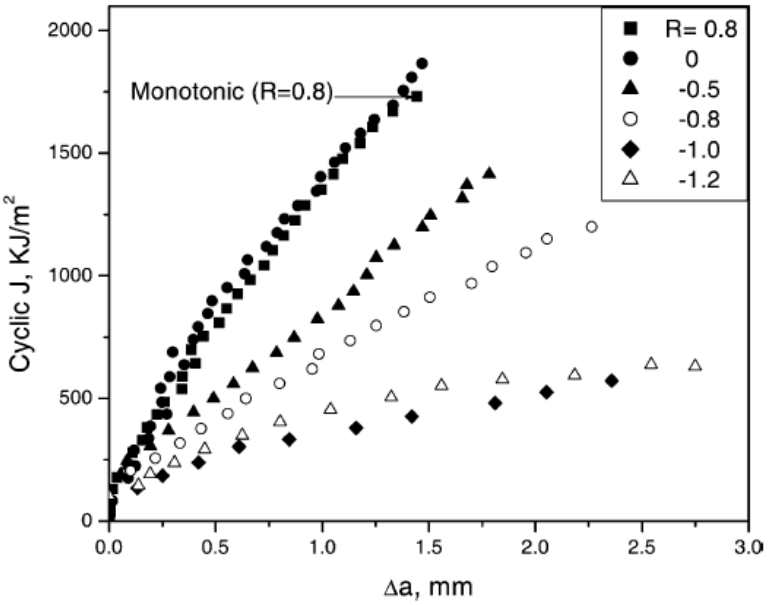

Figure 6.8: Fracture Resistance vs Load ratio ($\delta = 0.3$ mm) [9]

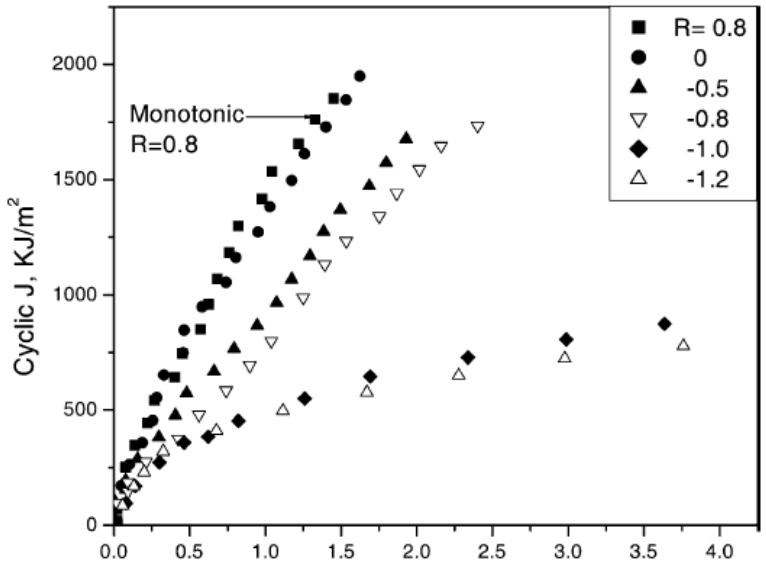

Figure 6.9: Fracture Resistance vs Load ratio ($\delta = 0.5$ mm) [9]

Experiment Conclusions

Cyclic loading can reduce the material fracture resistance compared to monotonic loading, especially the load ratio becomes negative.

An obvious observation is that, large crack tip blunting is observed under monotonic loading. However when the loading becomes cyclic, especially under a negative loading ratio, at the crack tip, more voids are sharpened due to the alternating tensile and compressive stresses [9]. As a result, it facilities the voids coalescence. And hence there is reduction on the fracture resistance at the crack tip region.

So under cyclic loading, if the load ratio is no less than zero, the fracture resistance will not be influenced. The tearing crack growth and fatigue crack growth can be treated separately and superposed in the end. While if the loading ratio becomes negative, the fracture resistance will be decreased. Especially near the crack tip, larger reverse plasticity zone will generate, the simplified superposition method is not suitable anymore, the mutual effects between the cyclic fracture resistance degradation and fatigue crack propagation should be careful considered [9].

6.3 Results Analysis

According to the previous FE study and the similar experiments, the analysis of this case is discussed below.

When the buckle arrestor goes on the first roller, the longitudinal strain at girth welding 12 o'clock position reaches 1.28%, ductile tearing growth happens. Based on the ECA, the predicted tearing crack growth in depth direction is 0.029 mm.

After that the buckle arrestor drops off and goes on the rollers repeatedly. During the cyclic loading, the reduction of the longitudinal strain is around 0.15% which is relatively small. So the reached CTOD will not be decreased during the later cyclic loading, no further tearing happens. For the later cycles, the accumulated fatigue crack growth is around 0.011 mm.

The final crack growth in depth direction can be treated as superposition of tearing crack growth and fatigue crack growth. It is about 0.04 mm which is within limit state. So the buckle arrestor will be safe under the current flaw size.

6.4 Future FE Study Proposal

6.4.1 Global Physics Summary

In the global physics point of view, when assessing the crack propagation, the three basic factors are: the crack driving force, the material fracture resistance, and the crack size.

For a defective structure, 1% strain is applied in the first cycle, tearing growth happens. During this stage, the applied crack driving force is compared with the fracture resistance curve which is usually obtained under the monotonic testing. Then in the following cycles, large cyclic strain range is acted on the flaw, as proved in experiments and FE simulation, high negative loading ratio could reduce the material fracture resistance.

In the later cycle, if the strain range is large enough, which means that the high negative loading ratio is applied. As a result, the degradation on the fracture resistance could cause further tearing growth. So the simplified superposition is not suitable anymore. The mutual effects between the ductile tearing and fatigue need

to be evaluated properly.

6.4.2 FE study Proposal

Gurson Model

Ductile fracture is the result of micro voids nucleation, growth and coalescence. The best known model is originally developed by Gurson and later modified by Tvergaard and Needleman. The Gurson model is a void growth model, by introducing the damage variable D into the void volume fraction. However the model is lack of a physical mechanism-based coalescence criterion [8]. Zhang et al. proposed a complete Gurson model by combining the GTN model with the Thomason's plastic limit load criterion [8]. An advantage of the complete Gurson model is that the critical volume fraction is not a material parameter anymore, it is determined by the plastic-limit load [8].

In previous Zhang et al. [8] FE study, the complete Gruson model is used to simulate the material fracture resistance under the pre-strain history. It is found out that the CTOD is influenced by the pre-strain history. Especially when the large compressive loading is added, there is degradation on the CTOD. As a consequence, further tearing growth happens in the next cycle. This FE simulation results are similar to the experiments which is conducted by P.K.Singh et al.[9].

In the fracture resistance testing, i.e. the monotonic testing, the resistance is measured under the stable crack growth situation, which means that the crack driving force rate is equal to the fracture resistance change rate. Thus in the FE simulation, within the stable condition, the obtained applied fracture resistance can be regarded as the material fracture resistance.

In Zhang et al. FE simulation, tearing growth happens when the large tensile strain is applied, the fracture resistance increases. After that during the unloading procedure, near the crack tip, the reverse plastic zone generates, as shown in Figure 6.10. Thus the calculated applied fracture resistance J_{app} is reduced due to the presence of the reverse plasticity. The higher compressive loading is applied, the lower fracture resistance will be obtained. Also due to the existence the reverse plastic zone, higher stress will be applied at the crack tip in the next cycle. So further tearing growth will happen in the next cycle.

In the future study, a FE study can be carried out based on the complete Gurson model [8] with the combination of the corresponding experiments. More cycles will be introduced to study the fracture resistance behavior under the large cyclic loading. Meanwhile the crack growth under the cyclic loading can be estimated through the FE simulation. All these procedure should be done under the stable crack growth condition. Otherwise the predicted fracture resistance curve will not be correct.

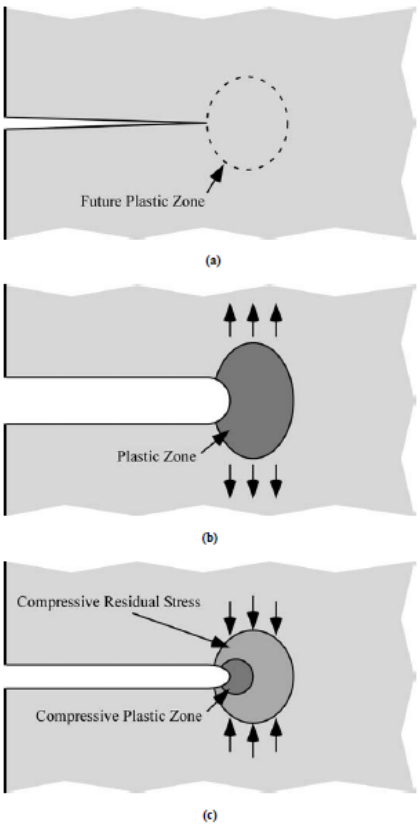

Figure 6.10: Deformation at the crack tip during cyclic loading [10]

Cohesive Zone in Combination with Gurson Model

The crack propagation can also modeled by combining the cohesive zone with the Gurson model, as shown in Figure 6.11. The Gurson model is used to describe the material behavior, the cohesive zone is used to model the crack propagation.

In the FE model, when defining the cohesive law, a master curve is applied initially, as shown in Figure 6.12. At the beginning, large strain is applied, and the crack grows. During the unloading stage, at the reverse plastic zone, there is degradation on the corresponding cohesive law. So in the next cycle, the cohesive law at the reverse plastic zone will follow another curve which has a lower bound. As for the degradation level, it is depend on the corresponding experiments.

The main idea of this FE model is to introduce the damage of the cohesive law to simulate the degradation of the fracture toughness at the reverse plastic zone. Though it can be realized by coupling the experiments data. However it is lack of physical meaning. Especially for the cohesive zone, it is more like a phenomenological model. Because the Gurson model can already present the ductile fracture failure mechanism. Also in reality, the crack propagation route is hard to predict.

While this model can be used to model the ductile-brittle transition region. In Geralf Hutter et al.[6] study, the Gurson model is used to describe the ductile failure mechanism, and the cohesive zone is used to model the cleavage fracture mecha-

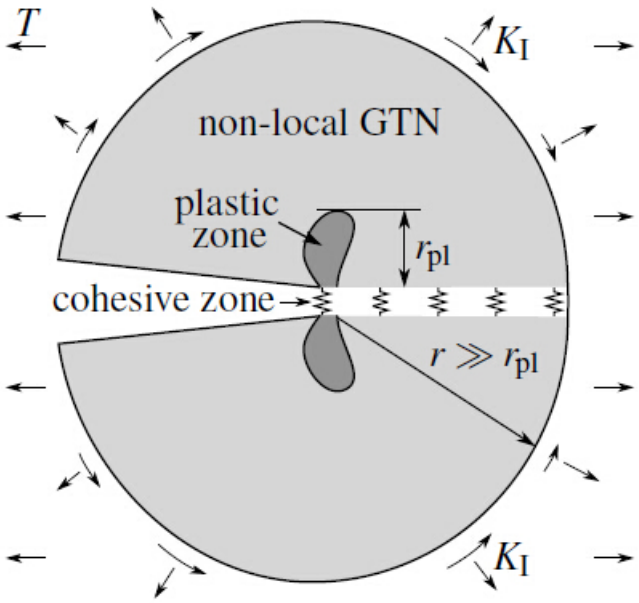

Figure 6.11: Model of crack propagation with cohesive zone and Gurson model [6]

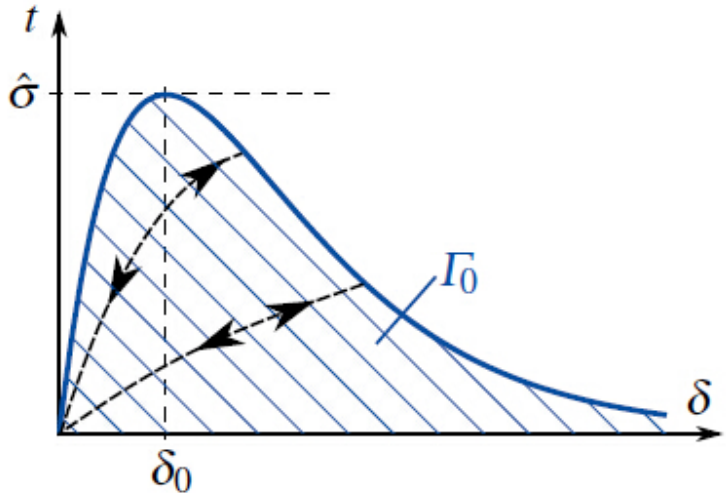

Figure 6.12: Cohesive Law [6]

nism. It is used to study the effects of the temperature on the fracture toughness. Because when the temperature is low, the cleavage failure contributes more; when the temperature is high, the ductile fracture becomes dominant.

In the present case, the cleavage fracture is not expected. The main objective is to model the ductile fracture under the large cyclic loading. The most suitable model for the ductile damage is the Gurson model. So the combination of the Gurson model and the cohesive zone is lack of physical meaning. Also the combination method could introduce more difficulties during the modeling, like the boundary conditions, mesh size, etc.

Chapter 7

Conclusions

A systematic study has been carried out on the buckle arrestor during its passage over the stinger, the main conclusions are summarized below.

A modified global FE model is implemented by using the displacement control method, and the result is similar to the static base model. However it gives better descriptions of the bending moment, the strain and the stress variations under a proper time loading history. Especially when the buckle arrestor suffers from the large cyclic loading, the typical static model will neglect the previous plastic deformation.

According to the previous similar FE study and the experiments, a common characteristic is found. During the cyclic loading, near the crack tip, the fracture resistance will be reduced if large compressive loading is added. The loading history effects on the fracture resistance should be considered. In this case, the cyclic loading range is relatively small. So the reached material fracture resistance remains unchanged in later cycles. No further ductile tearing growth happens and only fatigue crack growth is considered. In the end, the buckle arrestor will be safe during its passage over the stinger.

For a defective ductile structure under the cyclic loading, an accidental load could introduce tearing crack growth. While if cyclic loading range is relatively small, no large compressive loading is added, then no further tearing will happen in later cycles. The total crack growth can be regarded as the superposition of the tearing growth and fatigue growth. The present ECA can be used to predict the crack growth. If the cyclic strain range is quite large, for example a 0.5% strain range, the simplified superposition is not suitable anymore, the degradation on the material fracture resistance should be properly evaluated.

Bibliography

[1] Lorenzo Maria Bartolini and Lorenzo Marchionni et al., eds. *PIPE STRENGTH AND DEFORMATION CAPACITY: A NOVEL FE TOOL FOR THE NUMERICAL LAB. Proceedings of the OMAE 2014*. San Francisco, California, USA, 2014.

[2] *BS 7910. Guide to methods for assessing the acceptability of flaws in metallic structures*. 2013.

[3] *DNV-OS-F101. Submarine Pipeline System*. 2012.

[4] Ernst H. and Bravo RE et al., eds. *Strain history effects on fracture mechanics parameters-application to reeling. Proceedings of the OMAE 2005*. Halkidiki, Greece, 2005.

[5] R.J.H.Wanhill H.L.Ewalds. *fracture mechanics*. 1984.

[6] Geralf Hutter and Thomas Linse et al. "A Modeling Approach for the Complete Ductile-brittle Transition Region: Cohesive Zone in Combination with a Non-local Gurson-model". In: *International Journal of Fracture* 185 (2014), pp. 129–153.

[7] Giorgio Melis and Israel Marines-Garcia et al., eds. *Updates on Flaw Tolerability and Life of Offshore Double Joints in Strain-Based Loading Conditions. Proceedings of the Twenty-fifth International Ocean and Polar Engineering Conference*. Kona, Big Island, Hawaii, USA, 2015.

[8] P.A.Eikrem and Z.L.Zhang et al. "Numerical study on the effect of prestrain history on ductile fracture resistance by using complete Gurson model". In: *Engineering Fracture Mechanics* 75 (2008), pp. 4568–4582.

[9] P.K.Singh and V.R.Ranganath et al. "Effect of cyclic loading on elastic-plastic fracture resistance of PHT system piping material of PHWR". In: *International Journal of Pressure Vessel and Piping* 80 (2003), pp. 745–752.

[10] T.L.Anderson. *Fracture Mechanics. Fundamentals and Applications*. 2005.

[11] Heedo D. Yun and Ralf R. Peek et al., eds. *LOADING HISTORY EFFECT FOR DEEPWATER S-LAY OF PIPELINES. Proceedings of the OMAE 2003*. Cancun, Mexico, 2003.